

Electronic Raman Scattering in Superconductors as a Probe of Anisotropic Electron Pairing

T. P. Devereaux¹ and D. Einzel²

¹Department of Physics

University of California

Davis, CA 95616

²Walter Meissner-Institut für Tieftemperaturforschung

D-85748 Garching

Federal Republic of Germany

A gauge invariant theory for electronic Raman scattering for superconductors with anisotropic pairing symmetry is analyzed in detail. It is shown that Raman scattering in anisotropic superconductors provides a wealth of polarization-dependent information which probes the detailed angular dependence of the superconducting ground state order parameter. The Raman spectra show a unique polarization dependence for various anisotropic pair state symmetries which affects the peak position of the spectra and generates symmetry dependent low frequency and temperature power laws which can be used to uniquely identify the magnitude and symmetry of the energy gap. In particular, we calculate the collective modes and the subsequent symmetry dependent Raman spectra for a $d_{x^2-y^2}$ superconductor and compare our results to the relevant data on the cuprate systems as well as theoretical predictions for s-wave, anisotropic s-wave and s+id energy gaps. Favorable agreement is shown with the predictions for $d_{x^2-y^2}$ pairing and the experimental data on $\text{YBa}_2\text{Cu}_3\text{O}_{7-x}$, $\text{Bi}_2\text{Sr}_2\text{CaCu}_2\text{O}_8$ and $\text{Tl}_2\text{Ba}_2\text{CuO}_6$.

(Received December 31, 2021)

I. INTRODUCTION

Knowledge of the symmetry of the energy gap in superconductors provides a major step towards unraveling the puzzle of superconductivity in unconventional superconductors. While the evidence continues to accrue, the identification of the pair state in the heavy-fermion and cuprate systems has proven to be somewhat elusive [1]. While recent photoemission experiments [2] do allow for an angular-dependent determination of the gap and Josephson tunneling measurements have probed the phase of the gap [3], by far the most abundant information that has led to speculation of a non-BCS ground state has been focussed on the presence of power-laws in the low frequency and/or temperature behavior of transport and thermodynamic quantities [4]. However, due to the averaging over the entire Fermi surface, it is well known that the power-laws themselves do not uniquely identify the ground state symmetry of the order parameter but only can give the topology of the nodes of the energy gap along the Fermi surface, e.g., whether the gap vanishes on points and/or lines on the Fermi surface. Thus one cannot distinguish between different representations of the energy gap which have the same topology. For instance, for the case of d-wave tetragonal superconductors, there are two pure representations which have line nodes on the Fermi surface. Further, the energy gap can become smeared due to inelastic quasiparticle collisions, making a fully gapped superconductor seem like a one with gap nodes. While in principle the latter effect can be minimized by limiting the experiment to very low temperatures, the two-particle correlation functions determining the density, spin or current responses do not have the freedom to probe various portions of the gap around the Fermi surface, presenting a fundamental obstacle to uniquely identifying the pair state representation for the superconductor.

However, it is well known that Raman scattering has the ability to measure various degrees of freedom by simply rotating the incident and scattered photon polarization orientations. Formally, Raman fluctuations may be viewed as anisotropic mass fluctuations around the Fermi surface which do not obey a conservation law [5], such as, e.g., density fluctuations. While the isotropic density fluctuations between unit cells will be screened due to their coupling to long-range Coulomb forces, the intracell mass fluctuations can be anisotropic around the Fermi surface with no net charge and thus can be unscreened, providing a scattering mechanism for incoming photons.

The intensity of scattered light in a Raman experiment can be written in terms of a differential photon scattering cross section $\frac{d^2\sigma}{d\Omega d\omega} = \frac{d\sigma}{d\Omega} \frac{d\Omega}{d\omega}$ as

$$\frac{\partial^2}{\partial \omega \partial \omega'} = \frac{\omega_s}{\omega_i} r_0^2 S(\mathbf{q}; \omega);$$

$$S(\mathbf{q}; \omega) = \frac{1}{-[\omega + n(\omega)] \text{Im}}(\mathbf{q}; \omega); \quad (1)$$

Here $r_0 = e^2/mc^2$ is the Thompson radius, ω_i, ω_s is the frequency of the incoming and scattered photon, respectively, and we have set $\hbar = k_B = 1$. S is the generalized structure function, which is related to the imaginary part to the Raman response function through the fluctuation-dissipation theorem, the second part of Eq. (1). Finally $n(\omega) = 1/[\exp(\omega/T) - 1]$ is the Bose-Einstein distribution function. The generalization of the usual density-density correlation (S) and response (χ) functions to the case of Raman scattering can be generated by weighting the sums over momenta \mathbf{k} with the square of the Raman vertex $\Gamma(\mathbf{k})$.

For small momentum transfers and incident light energies smaller than the optical band gap (non-resonant scattering), the vertex for Raman scattering can be written in terms of the curvature of the energy band dispersion $\Gamma(\mathbf{k})$,

$$\Gamma(\mathbf{k}) = m \sum_{\mathbf{k}} e^{\mathbf{S} \cdot \frac{\partial^2 \epsilon(\mathbf{k})}{\partial \mathbf{k} \partial \mathbf{k}}} e^{\mathbf{I} \cdot \mathbf{k}}; \quad (2)$$

where $\mathbf{e}^{\mathbf{S} \cdot \mathbf{I}}$ denote the scattered and incident polarization light vectors, respectively, which select elements of the Raman tensor. The symmetry of the underlying crystal can be taken into account by expanding Γ in terms of a complete set of crystal harmonics Γ_L defined on the Fermi surface, i.e., [6]

$$\Gamma(\mathbf{k}) = \sum_{L, m} \Gamma_L^m \Gamma_L^m(\mathbf{k}); \quad (3)$$

where the index L represents the L th order contribution to the vertex which transforms according to the m th irreducible representation of the point group symmetry of the crystal. The quantum numbers L, m classify the anisotropy of the Raman fluctuations around the Fermi surface. The full \mathbf{k} -dependence is thus described by the addition of the basis functions (which become progressively more anisotropic for higher L) with different weights Γ_L^m . While the charge, spin, and current density response probes only a single L channel ($\Gamma(\mathbf{k}) = 1; L = 0$, for the charge and spin density, while $\Gamma(\mathbf{k}) = \mathbf{k}; L = 1$, for the current density), in principle all even L channels can contribute to the Raman vertex for bands which are non-parabolic. Thus by choosing the polarization light vectors accordingly, one can select different L, m channels which allow for different projections onto the Fermi surface. Therefore, electronic Raman scattering can provide detailed information which allows insight to the angular dependence of the pair-state symmetry.

In accord with this fact, the experimental results on the cuprate systems reveal a wealth of polarization dependent information that provides detailed evidence for determining the actual symmetry of the gap [7]. The existing body of data on the cuprate systems [8] reveal the main points: 1) in contrast to conventional superconductors such as Nb_3Sn , no clear well defined gap is seen for any polarization orientation even at the lowest temperatures measured ($T=T_c = 0.03$) [9], 2) the peak of the spectrum lies roughly at 30% higher frequency shifts for the polarization orientation which selects B_{1g} symmetry compared to all other symmetries [10-13], 3) there are indications that the temperature dependence of the peak in the B_{1g} channel follows more closely to a BCS form than any other symmetry [12], 4) the low frequency Raman shifts vary roughly as ω^3 for B_{1g} symmetries and linearly in ω for the others [9-13], and 5) the ratio of residual scattering in the superconducting state to the normal state is smallest for the B_{1g} case compared to all other configurations [13]. Such a rich spectrum of information should provide a stringent test for various candidates of the pairing symmetry states [14].

The purpose of the present paper is to investigate the polarization dependence of the Raman spectra for a superconductor in the weak coupling limit with anisotropic pairing symmetry. We calculate the electronic Raman scattering for a tetragonal superconductor at finite temperatures and for various polarization orientations in a gauge invariant manner and find a rich polarization dependence of the spectra that can be used to uniquely identify the energy gap. In particular, we examine the Raman response for s , d , $s+id$, and anisotropic s -wave superconductors and find that a $d_{x^2-y^2}$ state agrees surprisingly well with the current information on electronic Raman scattering in $\text{YBa}_2\text{Cu}_3\text{O}_{7-x}$, $\text{Bi}_2\text{Sr}_2\text{CaCu}_2\text{O}_{8-x}$ and $\text{Tl}_2\text{Ba}_2\text{CuO}_6$.

The plan of the paper is as follows: The ground work for the gauge invariant theory of electronic Raman scattering in anisotropic superconductors is reviewed in Section 2 using a kinetic equation approach. Section 3 concerns the connection of band structure to the Raman vertex and its relation to Fermi surfaces. Section 4 gives our results for the Raman response evaluated on a cylindrical Fermi surface for four types of energy gaps, i) s -wave, ii) d -wave, iii) $s+id$ -wave, and iv) a special type of anisotropic s -wave. Section 5 presents a comparison of the theory to the data on three cuprate systems and contains our conclusions. Appendix A deals with a solution of the weak coupling gap equation for the case of anisotropic gaps, Appendix B contains details of the theory for the case of (elastic or inelastic) quasiparticle scattering in the normal state, while lastly Appendix C is devoted to our calculations for the massive collective modes and the subsequent role of vertex corrections using a diagrammatic

approach. A brief account of our work has recently appeared [7].

II. KINETIC THEORY OF ELECTRONIC RAMAN SCATTERING IN ANISOTROPIC SUPERCONDUCTORS

A. Formalism

In this section we describe a kinetic equation approach for calculating generalized gauge invariant response functions in anisotropic superconductors, with the majority of our attention being focused on the electronic Raman response. Other formulations of the calculation are possible, and in particular a diagrammatic approach for the gauge invariant Raman response is discussed in detail in Appendix C. Since this approach has been discussed before by us [7], we will concentrate on the kinetic equation approach here.

We consider an anisotropic superconductor in which the electronic states are characterized by a momentum \mathbf{k} , an energy (band) dispersion $\epsilon_{\mathbf{k}} = \epsilon_{\mathbf{k}} + \epsilon_{\mathbf{k}}$ (with $\epsilon_{\mathbf{k}}$ the Fermi energy), a (band) group velocity $\mathbf{v}_{\mathbf{k}} = \nabla_{\mathbf{k}} \epsilon_{\mathbf{k}}$, an inverse effective mass tensor $M_{ij}^{-1}(\mathbf{k}) = \partial^2 \epsilon_{\mathbf{k}} / \partial k_i \partial k_j$, an energy gap $\Delta_{\mathbf{k}}$ and excitation energies $E_{\mathbf{k}} = [\epsilon_{\mathbf{k}}^2 + \Delta_{\mathbf{k}}^2]^{1/2}$. In global thermodynamic equilibrium such a system is described by a diagonal equilibrium phase space distribution function $n_{\mathbf{k}}^0$

$$n_{\mathbf{k}}^0 = \langle c_{\mathbf{k}}^\dagger c_{\mathbf{k}} \rangle = u_{\mathbf{k}}^2 f(E_{\mathbf{k}}) + v_{\mathbf{k}}^2 [1 - f(E_{\mathbf{k}})] = \frac{1}{2} [1 - \Delta_{\mathbf{k}} / E_{\mathbf{k}}] ; \quad (4)$$

with $\Delta_{\mathbf{k}} = (1/2E_{\mathbf{k}}) \tanh(E_{\mathbf{k}}/2T)$, $f(E_{\mathbf{k}})$ the Fermi function taken at the Bogoliubov quasiparticle energy $E_{\mathbf{k}}$ and the usual coherence factors $u_{\mathbf{k}}^2 = \frac{1}{2} [1 + \Delta_{\mathbf{k}} / E_{\mathbf{k}}]$ and $v_{\mathbf{k}}^2 = \frac{1}{2} [1 - \Delta_{\mathbf{k}} / E_{\mathbf{k}}]$ for particle-like and hole-like Bogoliubov quasiparticles. In a superconductor there exists in addition to the diagonal average $n_{\mathbf{k}}^0$ the off-diagonal average $g_{\mathbf{k}}^0$

$$g_{\mathbf{k}}^0 = \langle c_{-\mathbf{k}} c_{\mathbf{k}} \rangle = \Delta_{\mathbf{k}} / E_{\mathbf{k}} ; \quad (5)$$

The superconducting equilibrium energy gap is then determined from the self consistency equation

$$\Delta_{\mathbf{k}} = \sum_{\mathbf{p}} V_{\mathbf{k}\mathbf{p}} g_{\mathbf{p}}^0 ; \quad (6)$$

with $V_{\mathbf{k}\mathbf{p}} = \langle J_{\mathbf{k}\mathbf{p}} \rangle$ the pairing interaction.

Such a system is assumed to be subject to external perturbation potentials $U_{\mathbf{k}}^{\text{ext}}(\mathbf{q}; !)/\exp(i\mathbf{q} \cdot \mathbf{r} - i!t)$ which are generated in the usual way by an expansion of the Hamiltonian /

$(p - eA^{\text{ext}}/c)^2 = 2m + e^2 A^{\text{ext}}/c$ containing q and ω dependent scalar and vector electromagnetic potentials $A^{\text{ext}}(q; \omega)$ and $\mathbf{A}^{\text{ext}}(q; \omega)$, respectively, to second order in the vector potential (including $p \cdot \mathbf{A}$ terms):

$$\begin{aligned} U_k^{\text{ext}} &= e^2 A^{\text{ext}}/c + v_k \frac{e}{c} \mathbf{A}^{\text{ext}} + \frac{e^2}{c^2} \mathbf{A}_i^T \cdot \mathbf{M}_{ij}^{-1}(k) \cdot \mathbf{A}_j^S; \\ &= e^2 A^{\text{ext}}/c + v_k \gamma_1 + \gamma_2(k); \end{aligned} \quad (7)$$

where

$$\begin{aligned} \gamma_1 &= \frac{e}{c} \mathbf{A}^{\text{ext}}; \\ &= r_0 \mathbf{A}^T \cdot \mathbf{A}^S; \end{aligned}$$

$\gamma_2(k)$ denotes the Raman vertex given by Eq. (2). The last term in Eq. (7) can be interpreted to describe the scattering of an incident photon of frequency ω_i represented by the vector potential \mathbf{A}_i^T , into electronic excitations such as particle(hole, Bogoliubov quasiparticle or magnon pairs and an outgoing photon (Stokes process) of frequency $\omega_s = \omega_i - \omega$ (vector potential \mathbf{A}_j^S) with an associated total momentum transfer q .

The (linear) response of the distribution function $n_k(q; \omega) = n_k(q; \omega) - n_k^0$ in the absence of dissipation is given by the solution of the collisionless (particle(hole)symmetric) kinetic equation [15,16],

$$n_k = \frac{k}{\omega_k} (\omega_k - \omega) \omega_k + \omega_k (\omega + \omega_k) \frac{k}{2j_{-k} j_k}; \quad (8)$$

where $\omega_k = v_k q$,

$$\omega_k = \frac{\partial n_k^0}{\partial \omega_k} = \frac{j_{-k} j_k^2}{E_k^2} \omega_k + \frac{2}{E_k^2} \omega_k'; \quad (9)$$

and $\omega'_k = \partial f(E_k)/\partial E_k$. In addition we have defined

$$s_k = \frac{\omega_k \frac{\omega}{\omega_k} + s \omega_k \frac{\omega}{\omega_k}}{2j_{-k} j_k}; \quad s = \pm 1; \quad (10)$$

The cases $s = -1$ and $s = +1$ distinguish the coupling of the response of the pair-correlated electron system to phase and amplitude fluctuations of the order parameter, respectively, and will be discussed later. The quantity ω_k is the pair response function introduced by Tsuneto [17] which, in the limit $q \rightarrow 1$, with the coherence length, is given by,

$$\omega_k(q; \omega) = 4j_{-k} j_k^2 \frac{(\omega^2 - \omega_k^2) \omega_k + \frac{2}{4E_k^2} (\omega^2 - \omega_k^2)}{\omega^2 (\omega^2 - \omega_k^2) + \frac{2}{4E_k^2} (\omega^2 - \omega_k^2)}; \quad (11)$$

A more general expression for ϵ_k valid also for $1 < q < k_F$ is given in Ref. [18]. The total diagonal quasiparticle energy shift $\epsilon_k = \epsilon_k^+ + \epsilon_k^-$ may be decomposed into the sum of contributions even (+) and odd (-) with respect to the parity operation $k \rightarrow -k$. It differs in general from the contribution from the external potential U_k^{ext} through vertex corrections, or more physically, through electronic polarization potentials [19]. This fact may be expressed through the following diagonal self-consistency relation,

$$\epsilon_k = U_k^{\text{ext}} + 2 \sum_p (V_q + f_{kp}) n_p : \quad (12)$$

Here, $V_q = 4\pi e^2/q^2$ is the Fourier transform of the long-range Coulomb interaction and f_{kp} denotes the short-range Fermi liquid interaction the consequences of which are, however, not considered in what follows since we are interested in the limit of not too large q where the polarization correction from the long-range Coulomb interaction dominates the diagonal energy change.

The kinetic equation for the linearized odd diagonal distribution function $g_k(q;!) = g_k(q;!) - g_k^0$ reads

$$g_k + \epsilon_k + \frac{!^2}{4j_k j_k^2} \epsilon_k = \frac{y_k}{2j_k j_k} = \frac{k}{2j_k j_k} ! + \epsilon_k : \quad (13)$$

A straightforward variation of the equilibrium gap equation (6) leads to an odd diagonal self-consistency relation

$$\epsilon_k(q;!) = \sum_p V_{kp} g_p(q;!) ; \quad (14)$$

which can now be used to compute the odd diagonal energy shifts, namely the order parameter fluctuations $\epsilon_k(q;!)$ and $y_k(q;!)$. They represent the collective oscillations necessary to maintain gauge invariance, and must be determined self-consistently with the odd diagonal kinetic equation [15,16] (from which particle-hole asymmetric terms, which are typically of the order $O(T/T_F)$, with T_F the Fermi temperature, have been omitted),

$$\sum_p V_{kp} \frac{!^2}{4j_p j_p^2} = \sum_p V_{kp} \frac{!^+ + !^-}{2j_p j_p} : \quad (15)$$

In deriving (15) the equilibrium gap equation (6) has been used for simplification. In case of particle-hole symmetry, the density, current and Raman fluctuations do not couple to the quantity $!^+$, which represents the amplitude fluctuations of the order parameter. The physical significance of the quantity ϵ_k becomes clear in the (macroscopic) limit $! \rightarrow 0$,

in which only fluctuations of the phase of the superconducting energy gap determine the dynamics of the condensate and $\phi_k(q;!) = j_k \phi(q;!)$.

The important macroscopic observables, namely the density fluctuations $n_1(q;!)$, charge fluctuations $n_e(q;!)$, the Raman fluctuations $n(q;!)$ and the current fluctuations $j(q;!)$ are defined as

$$\begin{aligned} n_1(q;!) &= 2 \sum_k 1 - n_k(q;!); \\ n_e(q;!) &= 2 \sum_k e - n_k(q;!); \\ n(q;!) &= 2 \sum_k \epsilon_k n_k(q;!); \\ j(q;!) &= 2 \sum_k v_k [n_k(q;!) + \epsilon_k \phi_k(q;!)]; \end{aligned} \quad (16)$$

The factors of 2 arise from spin degeneracy.

We proceed with a solution of Eq. (15). For the time being we would like to restrict ourselves to the case where the pairing interaction factorizes as

$$V_{kp} = V \frac{k \cdot p}{2_0}; \quad (17)$$

This ansatz is sufficiently general to allow for an equilibrium gap function ϵ_k of arbitrary anisotropy in k -space. The maximum of such a gap is denoted ϵ_0 . ϵ_k is determined from the following form for the equilibrium gap equation (see Appendix A for further details),

$$\frac{1}{V} = \sum_{p \text{ shell}} \frac{j_p j_p}{2_0}; \quad (18)$$

Using Eq. (17), Eq. (15) can be solved immediately to give

$$\frac{\phi(q;!)}{2 j_k j} = \frac{i}{2} \phi(q;!) = \frac{P}{P} \frac{p \cdot p (1 + \frac{p \cdot p}{2_0})}{p \cdot p (1 + \frac{p \cdot p}{2_0})}; \quad (19)$$

The physical significance of the result (19) is that it describes the Goldstone mode for superconductors, the Anderson-Bogoliubov or gauge mode, i. e. the massless collective mode related to the spontaneously broken gauge symmetry. It is the existence of this mode which guarantees gauge invariance of the response theory or, equivalently, charge conservation, which we would like to briefly demonstrate now. For this purpose let us write the kinetic equation (8) in a form in which the lhs is reminiscent of the usual Landau-Silin equation [19],

$$i n_k - q \cdot k \psi n_k - \frac{\partial n_k^0}{\partial k} k = k [1 + \frac{k \cdot k}{2_0}] + k [1 + \frac{k \cdot k}{2_0}] \frac{k}{2 j_k j}; \quad (20)$$

Inserting Eq. (19), one observes that the r.h.s. of Eq. (20) vanishes upon summation over momenta k and the l.h.s. of (20) generates the continuity equation for the particle number density,

$$\sum_k \dot{n}_k - q \dot{j} = 0; \quad (21)$$

Hence we have demonstrated that accounting properly for the fluctuations of the phase of the order parameter leads to the conservation law for the (charge) density. Alternatively, one could argue in the following way: the phase fluctuation term ϕ_k on the r.h.s. of (20) can be thought of having its origin in a replacement of the scalar (ϕ^{ext}) and vector (A^{ext}) potentials in the first term on the r.h.s. of Eq. (20), representing the external potential contributions to ψ_k^+ and ψ_k , by their gauge-invariant counterparts

$$\begin{aligned} \phi^{\text{ext}} &\rightarrow \phi^{\text{ext}} - \frac{1}{c} \frac{\partial}{\partial t} \chi; \\ A^{\text{ext}} &\rightarrow A^{\text{ext}} + \nabla \chi; \end{aligned} \quad (22)$$

The phase variable χ characterizing this gauge transformation can then be fixed by the requirement of charge conservation, which, together with the trivial connection between χ and the order parameter phase fluctuation ϕ ,

$$\chi = \frac{2e}{c} \phi;$$

immediately leads to the result (19). This demonstrates clearly the equivalence of the existence of the Anderson-Bogoliubov mode with gauge invariance as well as the connection of gauge-invariance with the conservation law for the (charge) density.

Next we would like to demonstrate two simple consequences of a gauge-invariant formulation of superconducting response theory, namely those for the current response in the static ($\omega = 0$) and for the Raman response in the homogeneous ($q = 0$) limit. The static limit of the kinetic equation (20) reads

$$n_k \frac{\partial n_k^0}{\partial k} = -k \cdot k \sum_{p, p'} \frac{p \cdot p'}{p^2} \frac{p \cdot p'}{p^2} : \quad (23)$$

Integrating this according to the prescription (16) one gets the static (super) current response expressed in a generalized London formula:

$$\begin{aligned} j(q; 0) &= e j(q; 0) = \frac{e^2}{c} \langle \phi(q; 0) A^{\text{ext}}(q; 0) \rangle; \\ \langle \phi(q; \omega) \rangle &= \frac{q \cdot q}{q^2} \langle \phi(q; \omega) \rangle; \\ \langle \phi(q; \omega) \rangle &= 2 \sum_p \frac{v_p \cdot v_p}{\omega} \langle \phi(q; \omega) \rangle; \end{aligned} \quad (24)$$

Clearly, the second term in (24), sometimes referred to as backflow term [20], is necessary to maintain charge conservation in the general case of an anisotropic superconductor. Equivalently, it guarantees that the current is purely transverse in the static limit.

Let us now turn to the Raman response in the homogeneous limit. Here we may ignore terms linear in \mathbf{r}^{ext} and A^{ext} . For $q \neq 0$ the kinetic equation (20) assumes then the strikingly simple form

$$n_k = n_k^+ + \frac{P}{P} \frac{P}{P} \frac{P}{P}; \quad (25)$$

in which the second term on the r.h.s. originates from the order parameter phase fluctuations. The Coulomb interaction becomes irrelevant in this limit, as will become clear later, and we may write $n_k^+ = n_k$. The homogeneous Raman response of anisotropic superconductors can then be written in a form analogous to the London limit of the current response as

$$\begin{aligned} n(0;!) &= (0;!) - (0;!); \\ \chi_{ab}(q;!) &= \chi_{ab} - \frac{a_1 b_1}{11} (q;!); \\ \chi_{ab}(q;!) &= 2 \sum_p a_p b_p; \quad a_p, b_p = 1; \quad p: \end{aligned} \quad (26)$$

As in the case of the current response there is a "backflow" term (the second in the curly brackets), which guarantees charge conservation. This is easily seen in the limit of parabolic bands, where the Raman vertex χ_k is a constant and as a consequence the two terms in curly brackets cancel precisely. This is just another way of stating that there are no density fluctuations possible in the homogeneous limit $q \neq 0$ of a superconductor.

It is worth noting that there exists a homogeneous limit of the electronic Raman response also in normal metals when quasiparticle scattering processes are important characterized by a momentum {dependent lifetime τ_k . In Appendix B we show that an equation similar to (26) holds in the normal state with the Tsumeto function χ_k replaced by $\chi_k = (\epsilon_k^0 - \epsilon_k) (1 - i\tau_k)^{-1}$.

Let us now turn to a description of the Raman response at finite wavevector q . Our starting point will be Eq. (8) in which we select the even-parity contributions n_k^+ and $n_k^+ = n_0 + n_k$ with $n_0 = V_q n_1$:

$$\begin{aligned} n_k^+ &= [S_k + \frac{1}{2} k] n_0 + [k S_k + \frac{1}{2} k \frac{1}{11}] ; \\ S_k &= \frac{\frac{1}{2} k k}{\frac{1}{2} k} \frac{1}{k}; \end{aligned} \quad (27)$$

$$\epsilon^2 = \frac{\epsilon^2}{\epsilon^2} ; \quad \epsilon^2_q = \frac{q}{\epsilon_{11}} \epsilon^2$$

Integration over momenta k in Eq. (27) yields equations that describe the coupling of density and Ram an response:

$$\begin{aligned} n_1 &= \epsilon_{11}^{(0)} + \epsilon_1^{(0)} ; \\ n &= \epsilon_1^{(0)} + \epsilon^{(0)} ; \end{aligned} \quad (28)$$

where we have defined generalized (free) response functions

$$\epsilon_{ab}^{(0)} = \epsilon_{ab} + \frac{\epsilon^2_q}{\epsilon^2} \frac{\epsilon_{a1} \epsilon_{1b}}{\epsilon_{11}} + 2 \sum_p \left(\frac{\epsilon^2_p}{\epsilon^2} \frac{\epsilon_{p1} \epsilon_{1p}}{\epsilon_{11}} \right) a_p b_p : \quad (29)$$

The quantities $\epsilon_{ab}^{(0)}(q; \epsilon)$ are straightforward generalizations of the free superconducting Lindhard function which include vertices a_k, b_k . The Anderson-Bogoliubov collective mode causes the second term in the transverse contribution ϵ_{ab} (note that $\epsilon_{a1} = \epsilon_{1b} = \epsilon_{11} = 0$) and the longitudinal term which is characterized by the gauge mode frequency ϵ_q . Finally we explicitly work out the Coulomb renormalization $\epsilon_0 = V_q n_1$ which couples Ram an and density fluctuations and arrive at the following final result:

$$\begin{aligned} n &= \epsilon ; \\ \epsilon_{ab} &= \epsilon_{ab}^{(0)} - \frac{\epsilon_{a1} \epsilon_{1b}}{\epsilon_{11}^{(0)}} + \frac{\epsilon_{a1} \epsilon_{1b}}{\epsilon_{11}^{(0)}} \frac{1}{\epsilon} ; \\ &= 1 - V_q \epsilon_{11}^{(0)} : \end{aligned} \quad (30)$$

It should be noted that the Ram an response in superconductors in the small q limit in a form equivalent to Eq. (30) has first been derived by Klein and Dierker [21] using the Greens-function method. Our result from the kinetic equation method looks slightly different and, particularly, one can see that the Coulomb interaction acts so as to split the Ram an response into an unscreened "transverse" and a dielectrically screened "longitudinal" part, the latter being described by the full dielectric function of $\epsilon(q; \epsilon)$ of the superconductor in complete analogy to the behavior of the current response, discussed in Ref. [20]. Furthermore, an inspection of Eq. (30) shows, that all terms in the full response function ϵ_{ab} except are at least of the order $O(q^2)$, the last (longitudinal) term being even smaller, of the order $O(q^2 = 0)$. The role of the Coulomb interaction is thus limited to show up in terms of the order of at most $O(q^2)$ and is seen to be negligible in the homogeneous limit. The role of the collective Anderson-Bogoliubov mode, on the other hand, mainly consists of

providing a particle number conservation law. This manifests itself first in the correct mass fluctuation limit of Eq. (30), in which $\epsilon_k = \text{const}$ and all transverse terms vanish identically leaving essentially the screened RPA Lindhard response of the superconductor in which the collective mode gets shifted to the plasma frequency. Second it manifests itself in "partial screening" effects in the homogeneous limit of the Raman response, described by the second term of (30). These effects will be discussed in detail later.

B. Final Results for $q \rightarrow 0$.

Since $q \ll 1$ in the cuprates (with the coherence length), we are mostly interested in Raman scattering with vanishing momentum transfers. For such a case it is essential to conclude at this stage that the most important contribution to the electronic Raman effect in superconductors in the small q collisionless limit comes from the response function $\chi''(0; \mathbf{q}) = \lim_{q \rightarrow 0} \chi''(\mathbf{q})$. Physically, this function describes the photon-induced breaking of a Cooper pair into a pair of Bogoliubov quasiparticles with total momentum \mathbf{q} which is approximately zero.

Writing the Raman vertex as a sum $\chi(\mathbf{k}) = \chi_0 + \chi(\mathbf{k})$ of an isotropic and an anisotropic part (using Fermi surface harmonics $\chi(\mathbf{k}) = \sum_{L \neq 0} P_L(\mathbf{k})$), one may decompose the screened Raman response function at zero temperature in the limit of small momentum transfers as $\chi'' = \chi_k + \chi_q$ with

$$\begin{aligned} \chi_k &= \frac{[\chi_0^{(0)}]^2}{\chi_{11}^{(0)}} \frac{1}{q^2} = O\left(\frac{1}{q^2}\right); \\ \chi_q &= \chi''(0; \mathbf{q}) + O(q^2) \end{aligned} \quad (31)$$

into a longitudinal part χ_k , affected by (longitudinal) screening through the dielectric function of the superconductor, and a transverse part χ_q , independent of ϵ . Thus for $q \rightarrow 0$, only the transverse part of χ remains. We also see that in the case of the isotropic density vertex, $\chi(\mathbf{k}) = \chi_0$, the long range Coulomb forces completely screen the response and thus the only contribution to Raman scattering at $q = 0$ comes from energy bands with nonparabolic dispersion, i.e., the $L = 2$ and higher terms, representing intracell charge fluctuations.

Taking the limit of $q \rightarrow 0$ and carrying out the integration in the Tsuneto function, we obtain the final result for the Raman response at finite temperatures,

$$\chi''(q \rightarrow 0; i!) = \chi''(0; i!) - \frac{2}{1+i!} \frac{\chi_{11}^{(i!)}(i!)}{(i!)}; \quad (32)$$

where the spectrum of χ_{ab} is given by

$$\chi_{ab}^0(\omega) = \frac{N_F}{\omega} \tanh \frac{\omega}{4T} \text{Re} \left[\frac{1}{\omega} \int \frac{a(\mathbf{k})b(\mathbf{k})}{j(\mathbf{k})} d^3k \right] \quad (33)$$

where N_F is the density of states for both spin projections, Re denotes taking the real part, and \int denotes performing an average over the Fermi surface defined by

$$\int = \frac{\int_{\text{FS}} d^3k}{\int_{\text{FS}} d^3k} \quad (34)$$

The real part of χ_{ab}^0 is given as

$$\chi_{ab}^0(\omega) = \frac{1}{\omega} \int \frac{a(\mathbf{k})b(\mathbf{k})}{j(\mathbf{k})} d^3k \tanh \frac{\omega}{4T} ; \quad (34)$$

$$\chi_{ab}^0(\omega) = N_F \frac{j(\mathbf{k})}{\omega} \left[\frac{2}{j(\mathbf{k})^2} \arctan \frac{\omega}{j(\mathbf{k})} ; j(\mathbf{k}) > \omega ; \right. \\ \left. \frac{1}{j(\mathbf{k})^2} \log \frac{j(\mathbf{k}) + \omega}{j(\mathbf{k}) - \omega} ; j(\mathbf{k}) < \omega \right] .$$

This is the expression for the gauge invariant Raman response which has Coulomb screening and the Anderson-Bogoliubov gauge mode taken into account. It is also the form for the response calculated diagrammatically in the "pair approximation" for the bare bubble, modified with the usual RPA screening terms [21,22]. It does not take into account any vertex corrections resulting from the pairing interaction in other channels other than the pairing channel, as explained in the preceding discussion. We will refer back to this expression in the following Sections.

Important information can also be obtained from the temperature dependence of the response in the limit of zero frequency shifts, i.e., the static response. It can be shown that the ratio of the response in a superconductor to that of a normal metal in the limit of vanishing frequencies is given by the simple expression

$$\frac{\chi_{sc}^0(\omega \rightarrow 0)}{\chi_{ns}^0(\omega \rightarrow 0)} = \frac{2hf(\hat{k})}{h j(\hat{k})} ; \quad (35)$$

where f is a Fermi function [23]. This is an exact result which does not depend on vertex corrections and only depends appreciably on impurity scattering for nearly resonant impurity scatterers [23,24].

The important feature in all these expressions is that in general a coupling of the Raman vertex to the energy gap can occur under the momentum averaging over the Fermi surface. In all previous studies, this \mathbf{k} -dependence was either ignored or not fully exploited to determine

important information concerning the symmetry of the energy gap. This will be explicitly demonstrated in the following section where we evaluate these expressions for the screened Raman response for various pair state candidates and discuss its relevance to the cuprate materials.

We close this section by returning to the question of the presence of massive modes and vertex corrections (see above). In principle, the massive modes can lie at low frequencies and affect the low frequency behavior of correlation functions, and in particular, could even be used as a signal for a certain type of order parameter symmetry. We have carried out an analysis of the full gauge invariant calculation in the Appendix C for both cylindrical and spherical Fermi surfaces for a generalized pairing interaction. We identified the position of the collective modes as a function of coupling strength for a gap of $d_{x^2-y^2}$ (d_{xy}) representation using the notation of Sigrist and Rice, [25]) symmetry for both a spherical and cylindrical Fermi surface. Our conclusions are threefold: 1) the Goldstone modes do affect the Raman spectrum in the limit of $q \rightarrow 0$, in certain polarization symmetries (A_{1g}) where the "back flow term" in (32) is finite, 2) optical (massive) collective modes couple to a light probe only for case of a Fermi surface with z -dispersion for d -wave vertex corrections in the B_{1g} and E_g channels, 3) these modes are significantly damped and have a vanishing residue for those modes which lie at low energies. Therefore, the collective modes are of little importance to the Raman spectrum. These conclusions can be generalized to other energy gaps which have line nodes on the Fermi surface. Also, we discuss the role of the vertex corrections and find that while the overall shape of the spectra can be affected, the corrections are relatively minor. The details are contained in Appendix C, including a more general discussion of the role of vertex corrections. Therefore, we can conclude that Eqs. (32-35) give an adequate description of the Raman response.

III. BAND STRUCTURE, FERMI SURFACE AND THE RAMAN VERTEX FOR TETRAGONAL SYMMETRY

In this section we aim at providing a link between the Raman vertex and band structure for tetragonal crystals. In particular, we show how the choice of light polarization orientations results in selection rules for the symmetry components of the Raman tensor. In the first subsection we only consider scattering within a single band while we consider the case of multiple bands at the Fermi surface in the following subsection.

As we have seen in the previous section (see Eq. (2)), the Ramann tensor is directly related to the curvature of the band dispersion. In the following we limit our considerations to tetragonal materials which are relevant to high T_c superconductors. Although these materials possess orthorhombic distortions away from tetragonality, the selection rules for example from phonon scattering in the normal state seem to indicate that these orthorhombic distortions are small and that a tetragonal symmetry classification can be employed with little loss of generality. A simplest choice for the band structure which contains the basic physics of 2D like tetragonal systems with lattice constant a is given by,

$$\epsilon(\mathbf{k}) = -2t[\cos(k_x a) + \cos(k_y a)] + 4t^0 \cos(k_x a) \cos(k_y a) : \quad (36)$$

Here t and t^0 are the nearest and next nearest neighbor hopping parameters, respectively. This is the antibonding band derived from a reduction of a three band model [26], which gives by far the largest contribution to the density of states at the Fermi level for the cuprate systems [27]. The 2D Fermi surface is defined through the relation $\epsilon(\mathbf{k}) = \mu$, where μ is the chemical potential, which in turn determines the Fermi momentum,

$$k_F = k_F^{(0)} + \frac{\cos(\theta')}{\sin(\theta')} A : \quad (37)$$

The scalar prefactor $k_F^{(0)}$ can be expanded with respect to the fully symmetric basis functions (A_{1g} or Γ_1^+ using the notation of Sigrist and Rice [25]) for the tetragonal D_{4h} point group,

$$\begin{aligned} k_F^{(0)}(\theta') &= k_F^{(0)} + k_F^{(2)} \cos(4\theta') + k_F^{(4)} \cos(8\theta') + \\ &= k_F^{(0)} + \sum_{L=2, \text{even}} k_F^{(L)} a_L^0(\theta') : \end{aligned} \quad (38)$$

The higher order Fourier coefficients $k_F^{(L)}$ for $L > 0$ take into account deviations from cylindricity of the Fermi surface, $k_F^{(0)}$. The basis functions for the irreducible representations of the point group symmetry can be generalized as

$$a_L^j(\theta') = \cos(2L\theta' + \frac{j}{2}) ; \quad j \in \{0, 1, 2, \dots, L\} \quad (39)$$

where a_L^j transforms according to the A_{j+1g} symmetry, and

$$b_L^j(\theta') = \cos((2L-2)\theta' + \frac{j}{2}) ; \quad j \in \{0, 1, 2, \dots, L\} \quad (40)$$

which transform according to the B_{j+1g} {symmetry [29].

The Ram an tensor is given by

$$\begin{aligned} \hat{\mathcal{R}}(\mathbf{k}) &= m M_0^{-1}(\mathbf{k}) \\ &= 2m a^2 \begin{bmatrix} \cos(k_F x a) [t - 2t \cos(k_F y a)] & 2t^0 \sin(k_F x a) \sin(k_F y a) \\ 2t^0 \sin(k_F x a) \sin(k_F y a) & \cos(k_F y a) [t - 2t \cos(k_F x a)] \end{bmatrix} \end{aligned} \quad (41)$$

where $M_0^{-1} = \partial^2 \mathcal{E}(\mathbf{k}) / \partial k_x \partial k_y$. We denote matrices in k space (except the Pauli matrices) with a double arrow. We proceed to expand the Ram an tensor in quaternions,

$$\hat{\mathcal{R}}(\mathbf{k}) = m M_0^{-1}(\mathbf{k}) = \sum_{m=0}^3 \hat{\mathcal{R}}^{(m)}(\mathbf{k}) \tau^m; \quad (42)$$

with τ^m the Pauli matrices in $2D$ k space. The polarization light vectors select elements of the Ram an tensor according to

$$\hat{\mathcal{R}}(\mathbf{k}) = \hat{e}^I \hat{\mathcal{R}}(\mathbf{k}) \hat{e}^S = \sum_m (\hat{e}^I \tau^m \hat{e}^S) \hat{\mathcal{R}}^{(m)}(\mathbf{k}); \quad (43)$$

Next we expand the functions $\hat{\mathcal{R}}^{(m)}(\mathbf{k})$ in terms of Fermi surface harmonics

$$\hat{\mathcal{R}}^{(m)}(\mathbf{k}) = \sum_{L=2, \text{even}}^{\infty} \hat{\mathcal{R}}_L^{(m)}(\mathbf{r}'); \quad (44)$$

where

$$\hat{\mathcal{R}}_L^{(m)}(\mathbf{r}') = \begin{cases} a_L^0(\mathbf{r}'); & A_{1g} \quad (m = 0); \\ b_L^1(\mathbf{r}'); & B_{2g} \quad (m = 1); \\ a_L^1(\mathbf{r}'); & A_{2g} \quad (m = 2); \\ b_L^0(\mathbf{r}'); & B_{1g} \quad (m = 3). \end{cases} \quad (45)$$

The coefficients $\hat{e}^I \tau^m \hat{e}^S$ of the Ram an vertex can only assume the values 0 or 1 and have the following explicit form :

$$\hat{e}^I \tau^m \hat{e}^S = \begin{cases} [e_x^I e_x^S + e_y^I e_y^S]; & A_{1g} \quad (m = 0); \\ [e_x^I e_y^S + e_y^I e_x^S]; & B_{2g} \quad (m = 1); \\ [e_x^I e_y^S - e_y^I e_x^S]; & A_{2g} \quad (m = 2); \\ [e_x^I e_x^S - e_y^I e_y^S]; & B_{1g} \quad (m = 3). \end{cases} \quad (46)$$

We now can reconstruct the Ram an vertex (see Eq. (2)) as

$$\begin{aligned} \hat{\mathcal{R}}(\mathbf{k}) &= \sum_{L, m} \hat{\mathcal{R}}_L^{(m)}(\mathbf{r}') \\ &= \sum_L \hat{e}^I \tau^m \hat{e}^S \hat{\mathcal{R}}_L^{(m)}(\mathbf{r}'); \end{aligned} \quad (47)$$

We therefore see the connection between polarization orientation and symmetry. For example, if $\hat{e}^I = \hat{e}^S = \hat{x}$ are chosen, then a combination of A_{1g} and B_{1g} is selected. If $\hat{e}^I = \hat{e}^S = 2^{-1/2}(\hat{x} + \hat{y})$ then A_{1g} and B_{2g} symmetries are combined. These examples show in particular that A_{1g} symmetry cannot be individually accessed for in-plane polarizations, and subtraction procedures must be used.

B. Multi-sheeted Fermi surfaces

The above consideration can be easily adopted to the case of multiple energy bands contributing to the Fermi surface, for instance, due to the contribution of the chains as well as the planes in YBCO [27]. The total electronic Raman cross section for intraband scattering is just the sum of the contribution to the cross section for each band and thus results from the addition of the Raman response functions,

$$\chi_{\text{total}} = \sum_f \chi_f; \quad (48)$$

where χ_f denotes the contribution to the scattering from band f with an energy gap Δ_f for each band. The Raman vertex for each band is separately calculable in the same manner as in the previous section, and the same considerations there can be carried over to the multi-sheeted case trivially.

We draw the important point however that the contribution from each band will be weighted by the relative density of states and curvature of each band at the Fermi level. Therefore, for the case of the cuprates we believe that by far the largest contribution to electronic Raman scattering is thus arising from the single anti-bonding Cu-O layer band with the largest density of states and greatest curvature at the Fermi level. Further, it is not even clear whether an energy gap exists on the other energy bands (e.g., associated with the chains in YBCO), and if it does exist what symmetry it has. Therefore, we feel that to a very good approximation, the intraband scattering has a dominant contribution from the anti-bonding band. This is certainly the case for the single Cu-O layer compound, $Tl_2Ba_2CuO_6$.

We close this subsection with a discussion concerning interband scattering, or scattering from the anti-bonding band to another band near or at the Fermi level. In this case a separate theory is necessary to take into account the separate band dispersion and energy difference of the two bands, and the energy gap on each of the bands. This at present remains a future consideration. However, we remark at this point that once again this contribution

to the scattering cross section will be smaller than the contribution from scattering within the antibonding band due to the small curvature of the other energy bands and the value of the density of states at the Fermi level (again, the chains for example). Also, since the nature of the energy gap on the chains is completely unclear, we consider interband scattering to be beyond the scope of the present manuscript [28].

IV. PREDICTIONS FOR VARIOUS PAIR STATES

In this Section we evaluate Eqs. (32) and (33) for various pair states that are discussed in the literature as candidates to describe the pairing symmetry in the cuprates. We will first discuss the simple case of an isotropic gap and then discuss d-wave gaps (in particular, we will focus on the $d_{x^2-y^2}$ pairing symmetry) and then discuss gaps which are anisotropic but do not contain line nodes, e.g., an s -id and an anisotropic s -wave gap.

A. Isotropic s -wave

For the case of an angular independent gap, $\Delta(\mathbf{k}) = \Delta_0$, the Raman response is given by the simple BCS expression. It has the stereotypic features of BCS theory, namely, the existence of an energy gap threshold $2\Delta_0$ required to break a Cooper pair, and the ubiquitous square root divergence associated with the gap edge. We note in particular that the Raman vertex couples trivially to the energy gap and just determines an overall prefactor governing the Raman intensity. The vertex does not affect the lineshape and thus the spectrum is polarization independent apart from an overall prefactor. A polarization dependence can be generated in BCS theory by taking into account channel-dependent \mathbf{q} -state interactions [21] and/or impurity scattering [23], and accurate fits to the Raman data on A-15 superconductors can be obtained. However, for the most part this only produces an channel dependence in the vicinity of the gap edge and thus the main feature of the response is the uniform gap existing for all polarizations, which clearly cannot give an adequate description to the Raman spectra of the cuprate materials.

B. $d_{x^2-y^2}$ pairing

The explicit symmetry dependence of the spectra results due to a coupling of the energy gap and vertex when the energy gap is anisotropic. To demonstrate this, we now carry out

the averages over a cylindrical Fermi surface in Eq. (33) using a $d_{x^2-y^2}$ gap, $\langle \hat{k}; T \rangle = \rho_0(T) \cos(2\theta)$ (see Appendix A). We find that the Raman spectrum can be written down analytically in terms of complete elliptical integrals. Taking screening into account and defining $x = \sqrt{1 - 2\rho_0}$, we obtain for $T = 0$,

$$\frac{\omega_{B_{1g}}^{sc}}{2N_F \frac{2}{B_{1g}}} (q = 0; !) = \begin{cases} [(2 + x^2)K(x) - 2(1 + x^2)E(x)]; & x \leq 1, \\ x[(1 + 2x^2)K(1/x) - 2(1 + x^2)E(1/x)]; & x > 1, \end{cases} \quad (49)$$

$$\frac{\omega_{B_{2g}}^{sc}}{2N_F \frac{2}{B_{2g}}} (q = 0; !) = \begin{cases} [(1 - x^2)K(x) - (1 - 2x^2)E(x)]; & x \leq 1, \\ x[(2 - 2x^2)K(1/x) - (1 - 2x^2)E(1/x)]; & x > 1, \end{cases} \quad (50)$$

ie., the B_{1g} and B_{2g} channels are not affected by Coulomb screening. This is consistent with the mass fluctuations being only intracell in nature for these symmetry channels. However, the A_{1g} channel which contains both inter{and intracell} fluctuations is partially screened and is determined via

$$\omega_{A_{1g}}^{sc}(!) = \omega_{A_{1g}}^{nl}(!) - \frac{\frac{2}{A_{1g}} \omega_{1l}(!)}{\omega_{1l}(!)}; \quad (51)$$

with the spectral functions

$$\omega_{A_{1g}}^{nl} (q = 0; !) = \frac{2N_F \frac{2}{A_{1g}}}{15x} \begin{cases} [(7 - 8x^2 + 16x^4)K(x) - (7 - 12x^2 + 32x^4)E(x)]; & x \leq 1, \\ x[(11 - 28x^2 + 32x^4)K(1/x) - (7 - 12x^2 + 32x^4)E(1/x)]; & x > 1, \end{cases} \quad (52)$$

$$\omega_{A_{1g}}^{nl} (q = 0; !) = \frac{2N_F \frac{2}{A_{1g}}}{3x} \begin{cases} [(1 + 2x^2)K(x) - (1 + 4x^2)E(x)]; & x \leq 1, \\ x[(1 + x^2)K(1/x) - (1 + x^2)E(1/x)]; & x > 1, \end{cases} \quad (53)$$

and

$$\omega_{1l}^{nl} (q = 0; !) = \frac{N_F}{x} \begin{cases} [K(x) - E(x)]; & x \leq 1, \\ x[K(1/x) - E(1/x)]; & x > 1. \end{cases} \quad (54)$$

The real parts are obtainable through Kramers-Kronig transformation or numerically integrating Eq. (34). The response functions for finite T are obtained simply by multiplying Eqs. (49-54) by the factor $\tanh(\beta/4T)$. The partial screening of the A_{1g} channel arises technically from the observation that the square of the energy gap enters into the response function in Eq. (33). For the case of $d_{x^2-y^2}$ pairing symmetry, the energy gap squared contains a term

which transforms according to A_{1g} symmetry which leads to a finite overlap with the A_{1g} vertex in Eq. (32). This corresponds to partial "transverse screening" of the A_{1g} channel, and via this mechanism the intercell fluctuations are removed. Similar considerations hold if the gap were of another d{wave symmetry other than $d_{x^2-y^2}$.

These functions are plotted in Fig. (1) for the 3 symmetries indicated. We immediately see that the spectra is extremely polarization dependent, in contrast to the case of isotropic s{wave superconductors which is dominated by the square root divergence at the threshold in each channel. We see that the peak in the Raman spectra lies at different frequencies $\omega_{\text{peak}} \approx 2.0(T); 1.6(T)$ and $1.2(T)$ for the $B_{1g}; B_{2g}$ and A_{1g} channels, respectively [30]. The symmetry dependence of the spectra is a direct consequence of the angular averaging which couples the gap and Raman vertex, and leads to constructive (destructive) interference under averaging if the vertex and the gap have the same (different) symmetry. Thus it has been reasoned that the symmetry which shows the highest peak position gives an unique indication of the predominant symmetry of the gap [7]. The peak positions can be mildly affected by including interaction vertex corrections as discussed in Appendix C, with the net result being a slight upward shift of the peak location in the B_{2g} and A_{1g} channels. Also, while the presence of z{dispersion has little effect on the B_{1g} (apart from cutting off the logarithmic divergence) and B_{2g} channels, the A_{1g} peak position can be changed due to the addition of a term which has its main contribution at slightly lower frequencies. This effect is small provided that the Fermi surface is mostly cylindrical. We refer the reader to Appendix C for details.

The symmetry dependence is also manifest in the low frequency behavior, which can be written as

$$\begin{aligned}\chi''_{B_{1g}}(\omega \rightarrow 0) &= 3N_F \frac{2}{B_{1g}} x^3 = 4 + O(x^5); \\ \chi''_{B_{2g}}(\omega \rightarrow 0) &= N_F \frac{2}{B_{2g}} x^3 = 2 + O(x^3); \\ \chi''_{A_{1g}}(\omega \rightarrow 0) &= N_F \frac{2}{A_{1g}} x^3 = 2 + O(x^3);\end{aligned}\tag{55}$$

ie., the spectrum rises slower in the B_{1g} channel than the A_{1g} or B_{2g} channels, which have the same linear rise with frequency. The power laws are insensitive to vertex corrections and arise solely due to topology arguments. The appearance of power laws are a signature of an energy gap which vanishes on lines (points in 2D) on the Fermi surface. However, the channel dependence of the exponents are unique to a $d_{x^2-y^2}$ pair state. These channel-dependent power laws have been observed in the electronic contribution to Raman scattering in BSCCO [7,12], YBCO [11] and TBCO [13,31] and are strong evidence for a d{wave gap

of this symmetry as opposed to d_{xy} ; d_{xz} or d_{yz} symmetry, which also have nodes on lines on the Fermi surface [7,30].

We now investigate the temperature dependence of the theory and contrast to that of an isotropic s-wave superconductor. Using a weak coupling expression for the temperature dependence of the energy gap ($2\Delta_0 = T_c = 4.2794$) (see Appendix A), we numerically evaluate Eq. (35) for the temperature dependence of the normalized static response while taking screening into account. This function describes how the gap in the Raman spectrum at low energies opens up with cooling below T_c . The results are plotted in Fig. (2) as a function of T/T_c for a $d_{x^2-y^2}$ energy gap compared to a BCS isotropic gap. The low temperature behavior is given by a power law in T for all channels for the d-wave case while the ubiquitous exponential dependence in T is seen for all channels in the s-wave case. The power law behavior for the d-wave case is channel dependent, with exponents identical to those of Eq. (55), in the sense that Δ can be replaced by T . What is remarkable is that the fall off of the Fermi function at low temperatures is quite slow in those channels which are orthogonal to the symmetry of the gap, where the A_{1g} and B_{2g} channels show a residual broadening at $T=T_c = 0.3$ of roughly 20 percent of that of the normal state. This was argued in the case of electronic Raman scattering to be further evidence for an energy gap in the cuprate materials which has predominantly B_{1g} character, due to the observation that a gap opens up quickly in the B_{1g} channel compared to others channels which have been probed via Raman scattering [7].

As we have remarked before, since the Raman density response function only depends on the magnitude of the energy gap, it cannot be sensitive to the phase of the order parameter and thus cannot be directly used to determine if the gap changes sign around the Fermi surface. While the power law behavior at low frequencies and/or temperatures is indicative to the presence of nodes, in principle a very highly anisotropic order parameter with a small uniform gap everywhere on the Fermi surface could mimic the behavior of a gap with nodes when inelastic scattering or experimental resolution smears the threshold. In principle the detection of a threshold can then only be performed at very low temperatures where activated behavior can be observed. Since this remains a possibility we now discuss two types of energy gaps which are anisotropic but have a finite gap around the Fermi surface.

Kotliar and Joynt have suggested the possibility that an order parameter which is a superposition of an s-wave and a d-wave gap can also provide an adequate description to the various transport and thermodynamic measurements on the cuprate systems [32]. The s + id state has the interesting feature that in pure tetragonal superconductors there would be two transition temperatures associated with the formation of each gap separately. This is a consequence of the admixture of two different representations of the energy gap. However, orthorhombic distortions remove the $x \leftrightarrow y$ symmetry and thus A_{1g} and B_{1g} belong to the same representation. This leads then to one transition temperature. Since the orthorhombic distortions are quite small in the cuprates (judging from the observed phonons and selection rules), the transition temperature will be broad, which is in some conflict with the resistive transitions seen in the cuprates.

Nevertheless, we investigate what such a gap predicts for the Raman response by evaluating Eq. (33) on a cylindrical Fermi surface using a gap of the form $\Delta(\hat{k}) = \Delta_s(T) + i\Delta_d(T)\cos(2\theta)$. The results can be written again in an analytic form in terms of complete elliptical integrals. Taking screening into account and defining $x^2 = [(1/2)^2 - \Delta_s^2/\Delta_d^2]$, we obtain for $T = 0$,

$$\begin{aligned} \omega_{B_{1g}}^{sc} = \omega_{B_{1g}}(q = 0; !) = (x^2) \frac{4N_F \Delta_d^2}{3!} & \\ \times \left[(2 + x^2 + 3 \frac{\Delta_s^2}{\Delta_d^2}) K(x) - (2 + 2x^2 + 3 \frac{\Delta_s^2}{\Delta_d^2}) E(x); \quad x \leq 1, \right. & \\ \left. x[(1 + 2x^2 + 3 \frac{\Delta_s^2}{\Delta_d^2}) K(1-x) - (2 + 2x^2 + 3 \frac{\Delta_s^2}{\Delta_d^2}) E(1-x)]; \quad x > 1, \right. & \end{aligned} \quad (56)$$

$$\begin{aligned} \omega_{B_{2g}}^{sc} = \omega_{B_{2g}}(q = 0; !) = (x^2) \frac{4N_F \Delta_d^2}{3!} & \\ \times \left[(1 - x^2) K(x) - (1 - 2x^2 - 3 \frac{\Delta_s^2}{\Delta_d^2}) E(x); \quad x \leq 1, \right. & \\ \left. x[(2 - 2x^2 - 3 \frac{\Delta_s^2}{\Delta_d^2}) K(1-x) - (1 - 2x^2 - 3 \frac{\Delta_s^2}{\Delta_d^2}) E(1-x)]; \quad x > 1, \right. & \end{aligned} \quad (57)$$

$$\omega_{A_{1g}}^{sc}(i!) = \Delta_{1g} \Delta_{1g}(i!) \frac{\Delta_{1g}^2 (i!)}{1;1 (i!)}; \quad (58)$$

with the spectral functions

$$\omega_{A_{1g} \Delta_{1g}}(q = 0; !) = (x^2) \frac{4N_F \Delta_{1g}^2}{15!} \quad (59)$$

$$\begin{aligned}
& \left[(7 - 8x^2 + 16x^4 - 5 \frac{2}{s} = \frac{2}{d} (1 - 4x^2)) K(x) \right. \\
& \left. (7 - 12x^2 + 32x^4 - 20 \frac{2}{s} = \frac{2}{d} (1 - 2x^2)) E(x) \right]; \quad x < 1, \\
& x \left[(23 - 40x^2 + 32x^4 + \frac{5}{2} \frac{2}{s} = \frac{2}{d} x^2) (3 - 8x^2 + 8x^4) K(1=x) \right. \\
& \left. (11 - 28x^2 + 32x^4 - \frac{20}{2} \frac{2}{s} = \frac{2}{d} x^2) (1 - 2x^2) E(1=x) \right]; \quad x > 1,
\end{aligned}$$

$$\begin{aligned}
\omega_{A_{1g}}(q=0;!) = & (x^2) \frac{2^{p-2N_F} d A_{1g}}{3!} \\
& \left[(1 + 2x^2 + 3 \frac{2}{s} = \frac{2}{d}) K(x) \right. \\
& \left. (1 + 4x^2 + 6 \frac{2}{s} = \frac{2}{d}) E(x) \right]; \quad x < 1, \\
& x \left[(1 - 4x^2 + \frac{3}{2} \frac{2}{s} = \frac{2}{d} x^2) K(1=x) + \right. \\
& \left. (1 + 4x^2 + 6 \frac{2}{s} = \frac{2}{d}) E(1=x) \right]; \quad x > 1,
\end{aligned} \tag{60}$$

and

$$\omega_{B_{1g}}(q=0;!) = (x^2) \frac{2N_F d}{!} \left\{ \begin{aligned} & [(1 + \frac{2}{s} = \frac{2}{d}) K(x) - E(x)]; \quad x < 1, \\ & x [(1 - \frac{2}{s} = \frac{2}{d} x^2) K(1=x) - E(1=x)]; \quad x > 1. \end{aligned} \right. \tag{61}$$

The results are plotted in Fig. (3) using an value of $\frac{2}{s} = \frac{2}{d} = 0.25$. The finite gap $\frac{2}{s}$ is responsible for the threshold appearing at $2 \frac{2}{s}$, which is the minimum energy required to break a Cooper pair. The spectra are polarization dependent, with the B_{2g} and A_{1g} spectra displaying a discontinuous jump at the threshold while the B_{1g} channel shows a continuous rise from zero to a peak at $! = 2 \frac{2}{s} + \frac{2}{d}$. Since both the A_{1g} and B_{2g} channels exhibit broad maxima for the case of a pure $d_{x^2-y^2}$ gap, the presence of the $2 \frac{2}{s}$ threshold will imply a shifting of the peak of the spectra away from the pure case to values lower in frequency if $2 \frac{2}{s} < !_{peak}$ (or at least create a shoulder at $2 \frac{2}{s}$), while also removing any difference in the peak position between the A_{1g} and B_{2g} channels. Taken by itself this cannot be reconciled with the experimental data unless of course $\frac{2}{s}$ is very small.

D. Anisotropic s{wave pairing

Starting from band structure arguments, recently an anisotropic s{wave energy gap of the form

$$(\hat{K}) = \epsilon_0 + \epsilon_1 \cos^4(2') \tag{62}$$

has been proposed also to explain the cuprate materials [33]. This energy gap is anisotropic with predominantly B_{1g} like character but does not change sign around the Fermi surface.

This is one specific example of an anisotropic s-wave energy gap. While other representations for anisotropic s-wave gaps of course do exist (in particular, a possibility recently suggested by photoemission is $\epsilon(k) = \cos(k_x a) + \cos(k_y a) = \text{const.} + A \cos(4') / \cos^2(2')$ [34]), we remark that the response calculated here is not qualitatively different from other cases and thus address only this one case.

Again we evaluate the Raman response for such a superconductor numerically and plot our results for $\epsilon_0 = \epsilon_1 = 0.25$ in Fig. (4). Immediately we see similar behavior as in the previous case with one notable exception. While the spectra each show a $2\epsilon_0$ threshold, the B_{2g} channel displays a B.C.S.-like singularity at the threshold and the A_{1g} a large increase near the threshold that removes any trace of a peak-like structure in the spectra at higher frequencies. Again this would predict the same peak position (or a shoulder) for the A_{1g} and B_{2g} channels. Therefore, for ϵ_0 not too small, it is not possible using just the symmetry of the gap alone to arrive at a situation where the peaks in the Raman spectra in the A_{1g} and B_{2g} channels lie at separate high energies, again which is not in agreement with experiments.

In principle the s-wave component of the gap can be made vanishingly small. However, the greater anisotropy of the energy gap compared to the $d_{x^2-y^2}$ case leads to a further anisotropy of the position of the peaks in each channel, with peaks in the spectra at $\omega = 2\epsilon_{\text{max}}; 0.6\epsilon_{\text{max}}; \text{ and } 0.2\epsilon_{\text{max}}$ for the $B_{1g}; B_{2g}; \text{ and } A_{1g}$ channels, respectively, where $\epsilon_{\text{max}} = \epsilon_0 + \epsilon_1$. On top of this, the low frequency power-law behavior is linear in each channel, in contrast to the $d_{x^2-y^2}$ results. This is a general feature that the spectra become more and more polarization dependent the greater the anisotropy of the energy gap (compare to Fig. (1) for the $d_{x^2-y^2}$ case).

V. COMPARISON WITH DATA ON THE CUPRATE SYSTEMS AND CONCLUSIONS

In this Section we present a comparison of the theory for a $d_{x^2-y^2}$ paired superconductor to recent measurements on the electronic Raman continuum in three cuprate superconductors. In what follows, we plot $S(\omega)$, Eq. (1), which is given by χ'' of Eqs. (49)–(54) multiplied by the Bose factor. In drawing the fits to the spectra, the following procedure is employed. First the fit to the B_{1g} spectrum is made which determines the maximum value of the energy gap ϵ_0 via the position of the peak in the spectrum. Next, the derived response is convoluted with a Gaussian which mimics the effect of finite z -dispersion of the Fermi surface, experimental resolution, inelastic scattering, etc. Once this is done, the parameters

remain fixed and only the prefactor of the vertex is left to be adjusted to match the overall intensity, which has no effect on the lineshape. Since this is in principle derivable from band structure but presently unknown even for such simple metals as Aluminum, this remains a free parameter.

We first fit the data taken on single crystals of as grown $\text{Bi}_2\text{Sr}_2\text{CaCu}_2\text{O}_8$ ($T_c = 90\text{K}$) obtained in Reference [12] for all symmetries at $T = 20\text{K}$, where a subtraction procedure has been employed to ascertain the A_{1g} signal (see Section 2.2). The comparison of the theory with experiment is shown in Fig. (5). The parameters used to obtain the best fit to the spectrum are $\omega_0 = 287\text{ cm}^{-1}$ and a smearing width of $\gamma_0 = 0.15$. The theory gives good agreement with the data at low frequency shifts while at higher frequency shifts the theory fails to produce the broad continuum which is relatively constant up to the scale of an eV. This is most likely due to the neglect of impurities and/or electron-electron scattering [35], which is beyond the scope of the paper. We see immediately that the peak positions in the B_{2g} and A_{1g} channels given by the theory automatically agree with the data. Also the asymptotic behavior of the continuum at low frequencies given by Eq. (33) is shown in the data when one neglects the phonons at roughly 100 and 330 wavenumbers. Again, these power laws are intrinsic to a $d_{x^2-y^2}$ pair state. Lastly, the ratio of the intensity of the spectra in different channels is consistent with Eq. (35) and Fig. (2), which predicts that the B_{1g} channels show the smallest intensity at low frequencies while the A_{1g} channels show the largest. All of the experimental features are thus consistent with the theory at least at low frequency shifts $\omega < 1000\text{ cm}^{-1}$.

We now turn to the data taken on single crystals of $\text{YBa}_2\text{Cu}_3\text{O}_7$ ($T_c = 88\text{K}$) obtained in Ref. [11] for all symmetries at $T = 20\text{K}$, where the same subtraction procedure used in BSCCO was employed to ascertain the A_{1g} signal. The comparison of the theory to the data is shown in Fig. (6), with the parameters $\omega_0 = 210\text{ cm}^{-1}$ and $\gamma_0 = 0.2$. Again, the theory gives a good description of the data for $\omega < 1000\text{ cm}^{-1}$. We again see the peak positions at relatively the same place as in BSCCO, and power laws linear in frequency at low shifts for the B_{2g} and A_{1g} channels. We note that while the cubic rise of the spectra predicted by the theory fits rather well with the B_{1g} data in BSCCO, we remark that the Fano effect of the B_{1g} phonon which appears to be stronger in YBCO than in BSCCO can obscure the rise of the spectra at low frequencies and give the appearance of a linear dependence on frequency [36]. Lastly, the ratios of the response in the static limit again are consistent with the theory.

Lastly, we investigate the single layer Thallium compound $\text{Tl}_2\text{Ba}_2\text{CuO}_6$ ($T_c = 80\text{K}$) obtained in Ref. [13]. The sample is most likely the most affected by disorder and therefore

our theory will not be expected to give the best fit to the data. Our fits is shown in Fig. 7 for the B_{1g} and the mixed $A_{1g} + B_{2g}$ channels at $T = 20K$, where we have ignored the contribution from the B_{2g} channel since it is believed to be minor compared to A_{1g} . The value of the parameters used are $\omega_0 = 232\text{cm}^{-1}$ and smearing width $\Gamma_0 = 0.25$. All phonons have been subtracted. Once again the theory gives a good description of the relative peak positions. Considering also that this compound has only one Cu-O layer, the agreement of the theory with experiment also validates the assumption that the Raman scattering results predominantly from intraband fluctuations of the single Cu-O layer band, and that interband scattering can be neglected. The theory also accounts for the linear rise of the spectrum for the A_{1g} channel for low frequencies. However, the theory cannot account for the linear rise of the spectrum in the B_{1g} channel. This most likely is due to the neglect of impurity scattering. The residual scattering near zero frequency shifts is also borne out by the theory, although the amount is underestimated for the B_{1g} channel. Again, this most likely has to do with the neglect of impurity scattering.

We remark that the theory is incomplete in that the theory fails to describe the $\omega \rightarrow 0$ continuum at large frequency shifts. Moreover, the theory cannot be extended to the normal state since the response functions vanish at T_c in the limit $q \rightarrow 0$ due to phase space restrictions. Here the additional physics of electron-electron scattering and/or impurity scattering must be incorporated to have a consistent theory to simultaneously describe the normal and superconducting state data. This remains a topic of further research [24]. Nevertheless, the low frequency behavior of the spectra, and in particular, the relative peak positions of each polarization channel are quantitatively described by the theory.

Thus we have seen that the Raman measurements on the cuprate systems provide a large body of symmetry dependent information all of which agrees with the predictions of $d_{x^2-y^2}$ pairing. Of course at present the information from Raman alone cannot completely rule out the possibility of the presence of a very small gap which exists over the entire Fermi surface nor can it determine whether the gap changes sign around the Fermi surface. However, the theoretical comparison shows that the gap must be predominantly of B_{1g} character, and the low temperature and low frequency data seem to indicate that the s-wave component of the gap must be very small if it exists at all. More precise measurements could of course clarify this point further. Also, more work is needed from band structure to pin down magnitude of the Raman tensor elements to predict the overall intensities.

ACKNOWLEDGMENTS

The authors would like to thank Drs. R. Hackl, G. Kug, R. Nemetschek and B. Stadlber for providing us with their data and discussions. Similarly, we thank D. Reznik, R. T. Scalettar, A. Virostek, A. Zawadowski, and G. T. Zimanyi for enlightening discussions. This work was supported in part by NSF Grant number 92-06023 and by the American Hungarian Joint Grant Number NSF 265/92b. One of the authors (T.P.D.) would like to acknowledge the hospitality of the Walter Meissner Institute, the Research Institute for Solid State Physics of the Hungarian Academy of Science, and the Institute of Physics of the Technical University of Budapest where parts of this work were completed.

APPENDIX A: WEAK COUPLING RESULTS

In this appendix we want to show that a gap anisotropy causes both the gap at zero temperature $\Delta_0(0)$ and the specific heat discontinuity at the transition $C=C_N$ (related to the slope of the gap function near T_c) to deviate from their respective BCS values of $(\Delta_0(0)=T_c)_{BCS} = \exp(-\gamma) = 1.7638...$ and $(C=C_N)_{BCS} = 12\pi^2\gamma(3) = 1.4261...$, with $\gamma = 0.57721...$ and $\gamma(3) = 1.20205...$ denoting Euler's constant and Riemann's zeta function respectively. A straightforward solution of Eq. (18) leads to

$$\frac{\Delta_0(0)}{T_c} = \frac{\Delta_0(0)}{T_c} \exp \frac{\langle \sum_p \Delta_p^2 \ln(\Delta_p \mp \Delta_0) \rangle_{FS}}{\langle \sum_p \Delta_p^2 \rangle_{FS}} ;$$

$$\frac{C}{C_N} = \frac{C}{C_N} \frac{\langle \sum_p \Delta_p^2 \rangle_{FS}^2}{\langle \sum_p \Delta_p^4 \rangle_{FS}} ; \quad (A1)$$

These results may be used to generate an interpolation formula for the temperature dependence of the gap maximum $\Delta_0(T)$:

$$\Delta_0(T) = \Delta_0(0) \tanh^4 \frac{1}{2} \frac{\sum_p \Delta_p^2}{\sum_p \Delta_p^4} \frac{3}{2} \frac{C}{C_N} \frac{\Delta_0^2}{\langle \sum_p \Delta_p^2 \rangle_{FS}} \frac{T_c}{T} - 1.5 ; \quad (A2)$$

For the special case of a gap with $d_{x^2-y^2}$ symmetry, one obtains for the parameters $\Delta_0(0)$ and $C=C_N$ the following numbers:

$$\Delta_0(0) = \begin{cases} \frac{8}{\pi} \exp \left(-\frac{16}{15} \right) = 2.5626; & \text{spherical FS,} \\ \frac{8}{\pi} \exp \left(-\frac{1}{2} \right) = 2.1397; & \text{cylindrical FS,} \end{cases}$$

$$C/C_N = \begin{cases} \frac{12}{7} \frac{7}{(3)15} = 0.6655; & \text{spherical FS,} \\ \frac{12}{7} \frac{2}{(3)3} = 0.9507; & \text{cylindrical FS.} \end{cases}$$

We should emphasize, that these numbers should not be taken too seriously since they emerge from a weak coupling treatment. One should rather adopt the convention to treat them as parameters which can be adjusted to experiment and so account for strong coupling effects in the trivial sense in which they appear as renormalizations of the quantities ϵ_0 and $C = C_N$.

APPENDIX B: IMPURITY SCATTERING IN THE NORMAL STATE

In this Appendix we would like to demonstrate that the normal state electronic Raman response has a nonvanishing $q \rightarrow 0$ limit in the presence of quasiparticle collisions. In the collisionless limit of a superconductor, the quantity χ'' has a finite value in the normal state limit $\epsilon_0 \rightarrow 0$ only at finite wavenumbers q . The normal state Raman response can persist in the limit $q \rightarrow 0$ however if one assumes (elastic or inelastic) scattering processes to take place. These scattering processes may be generally introduced through a collision integral \mathcal{I}_k in the normal state kinetic equation [19],

$$\begin{aligned} i\hbar \partial_t n_k - q_k v_k \hbar k &= i \mathcal{I}_k f_{\mathbf{k}} g; \\ \mathcal{I}_k f_{\mathbf{k}} g &= \frac{1}{\hbar} h_k + 2 \sum_p C_{kp} h_p; \\ h_k &= n_k \frac{\partial n_k^0}{\partial \epsilon_k} \epsilon_k; \end{aligned} \quad (\text{B1})$$

The structure of the collision integral depends on the scattering mechanism that one is interested in and is, in many cases, subject to an approximate treatment of the collision operator C_{kp} . However, such approximations have to be consistent with the requirement of charge conservation [37,38,39]. An approximation with this property is the separate kernel approximation [40],

$$C_{kp} = \frac{\partial n_k^0}{\partial \epsilon_k} \epsilon_0 \frac{1}{\hbar} \frac{1}{\epsilon_k - \epsilon_p} \left(2 \sum_p \frac{\partial n_p^0}{\partial \epsilon_p} \epsilon_p \right)^{-1} : \quad (\text{B2})$$

The scattering processes are here represented by a momentum (dependent) quasiparticle lifetime ϵ_k and a scattering parameter ϵ_0 . The continuity equation is obtained from Eq. (B1) by summing over momenta k ,

$$i\hbar \partial_t n - q \cdot j = \sum_p 2i \frac{h_p}{\epsilon_p} (1 - \epsilon_0) :$$

Particle number conservation is therefore connected with the choice of the scattering parameter $\epsilon_0 = 1$. One may show that the normal state Raman response in the $q \rightarrow 0$ limit assumes form equivalent to the result (26) for the pair breaking Raman effect:

$$\lim_{\omega \rightarrow 0} \lim_{q \rightarrow 0} \left(\frac{1}{\omega} \right) = \frac{1}{\omega} \left(\frac{1}{\omega} \right);$$

$$\chi_{ab} = 2 \sum_p \frac{\partial n_k^0}{\partial \epsilon_k} \frac{a_p b_p}{1 - i\tau_p} : \quad (B3)$$

Like in the superconducting case, the projected structure of Eq. (B3) has its origin in the particle number conservation law. This result can be applied to impurity or phonon scattering as well as to inelastic two-particle scattering and requires the specification of the momentum-dependent quasiparticle lifetime for each of these cases.

APPENDIX C: DIAGRAMMATIC GAUGE INVARIANT RAMAN RESPONSE: ROLE OF VERTEX CORRECTIONS AND COLLECTIVE MODES

In this Appendix we derive expressions for gauge invariant generalized correlation functions using a diagrammatic approach with the main emphasis placed on electronic Raman scattering. After solving the coupled integral equations for the renormalized vertex, we evaluate the position, broadening and residue of the massive and massless collective modes as a function of coupling strength for a $d_{x^2-y^2}$ energy gap on a spherical Fermi surface. We then investigate the collective modes on a cylindrical (2-D) Fermi surface by tuning on any z -dispersion in the band structure.

We begin by writing down the expression for the general two-particle response function in Nambu space as

$$\chi(q; i\omega) = T \sum_{i\omega_n} \text{Tr} [\hat{\chi}(k; q; i\omega) \hat{G}(k + \frac{q}{2}; i\omega_n) \hat{\chi}(k - \frac{q}{2}; i\omega_n - i\omega)]; \quad (C1)$$

$$\hat{\chi}(k; q; i\omega) \hat{\chi}(k; q) = T \sum_{i\omega_n} \sum_{p, p^0} \hat{G}(p + \frac{p^0}{2}; i\omega_n) \hat{\chi}(p; p^0; i\omega) \quad (C2)$$

$$\hat{G}(p + \frac{p^0}{2}; i\omega_n) V(p - k + \frac{q}{2}; k - p + \frac{q}{2}, \frac{p^0}{2}) \hat{G}(p - \frac{p^0}{2}; i\omega_n - i\omega)$$

where Tr denotes taking the trace, τ_i are Pauli matrices in Nambu space, and the vertex $\hat{\chi}$ determines the correlation function of interest. The dressed vertex $\hat{\chi}$ contains the interactions V responsible for maintaining gauge invariance.

Our consideration is focused on the Raman vertex which describes the anisotropic mass fluctuations, $\hat{\chi}(k; q) = \chi_3(k)$ with the limit of small q taken. Other choices of the vertices are

$$\begin{aligned}
\chi(k) &= \chi_3; & \text{charge density;} \\
\chi(k) &= \chi_0; & \text{spin density;} \\
\chi(k) &= k_0; & \text{current density;}
\end{aligned}
\tag{C 3}$$

Thus from Eqs. (C 3) we see that while the spin and charge density vertices probe only the $L = 0$ channel and current density probes $L = 1$, in principle all even L channels contribute to the Raman vertex. In fact the charge density is the first term in the expansion of the Raman vertex.

If one replaces the dressed vertex by the undressed one, Eq. (2), then of course Eq. (C 1) is manifestly not gauge invariant, and in general the neglect of collective modes arising from a gauge invariant treatment could in principle affect the overall spectrum. Usually the question of gauge invariance is rather an academic one since the modes that appear in BCS systems have little impact on the response functions of a superconductor. It is well known that due to the spontaneously broken $U(1)$ gauge symmetry in s-wave superconductors, two collective modes appear { an optical one with a frequency of 2Δ which is damped { and a sound-like mode, the Anderson-Bogolubov mode, which is soft and lies in the gap for neutral superconductors but is raised to the plasmon energy by the long range Coulomb forces via the Higgs mechanism. However, in unconventional superconductors, there can exist in principle additional Goldstone modes corresponding to the additional broken continuous symmetries such as SO_3^S spin rotational symmetry in spin-triplet systems plus SO_3^L orbital rotational symmetry in spin-singlet systems if the gap does not possess the full symmetry of the Fermi surface. In addition, massive collective modes can arise if the energy gap is degenerate or has an admixture of different representations from the point group. The massive modes can in principle lie below the gap edge and thus be relevant for the low frequency dynamics of correlation functions. For example, the spectrum of collective modes in ^3He is well known in both phases and lead to observable effects [16]. However, the collective modes of possible d-wave states that might be candidates for strongly correlated systems are not as well understood [41]. There are indications that a d-wave state of $d_{x^2-y^2}$ is particularly favorable in systems with strong correlations [42], thus underscoring the necessity of an understanding of the response functions and collective modes for such a superconductor.

We continue our calculation for the gauge invariant Raman response by first expanding the renormalized matrix vertex $\hat{\chi}$ along the Fermi surface in terms of crystal harmonics,

$$\hat{\chi}(\hat{k}; i!) = \sum_{L, m} \hat{\chi}_L^m(i!) \chi_L^m(\hat{k});
\tag{C 4}$$

and do the same for the pairing interaction,

$$V(\hat{\mathbf{k}}; \hat{\mathbf{p}}) = \sum_{L, \mu L^0, m, m^0}^X V_{L, \mu L^0}^{m, m^0}(\hat{\mathbf{k}}) \frac{m^0}{L^0}(\hat{\mathbf{p}}): \quad (\text{C } 5)$$

The integralequation for the renormalized vertex at $q = 0$ can then be written as

$$\hat{\Lambda}_L^m(i!) = \frac{TN_F}{2} \sum_{i!_n}^X \int d^0 \sum_{L^0, \mu L^0, m^0, m^{\infty}}^X V_{L, \mu L^0}^{m, m^0} \quad (\text{C } 6)$$

$$h_{L^0}^{m^{\infty}}(\hat{\mathbf{k}}) \frac{m^0}{L^0}(\hat{\mathbf{k}}) {}_3\hat{G}(\hat{\mathbf{k}}; i!_n) i! \hat{\Lambda}_{L^0}^{m^{\infty}}(i!) \hat{G}(\hat{\mathbf{k}}; i!_n) {}_3i;$$

where $h_{L^0}^{m^{\infty}}(\hat{\mathbf{k}})$ denotes an average over the Fermi surface and $i!$ denotes the density of states at the Fermi level. Eq. (C 6) is completely general for any type of vertex, interaction and gap symmetry. In particular, for the case of an isotropic energy gap, Eq. (C 6) recovers the previous results for the density, current [43], and Raman responses [21]. We confine ourselves to the case of singlet energy gaps and use the BCS approximation,

$$\hat{G}(\mathbf{k}; i!_n) = \frac{i!_n + {}_3 + (\hat{\mathbf{k}})_1}{(i!_n)^2 E^2(\mathbf{k})}; \quad (\text{C } 7)$$

where $E^2(\mathbf{k}) = {}^2 + {}^2(\hat{\mathbf{k}})$. More complicated Green's functions could be treated with the same scheme. However, the analysis gets considerably more complicated and cannot be carried as far analytically.

In general the pairing interaction V can have off-diagonal as well as diagonal terms in the L basis, and in general all channels will be coupled. If the interaction has the symmetry of the Fermi surface then the integral equations only couple different channels L and L^0 which transform according to the same irreducible representation. However, the subsequent matrix can be diagonalized with respect to the indices of the same representation resulting in a new set of basis functions which are linear combinations of the old basis functions of the same representation in different L channels [44]. Thus we can then write the interaction as a diagonal matrix in the new basis functions which still has a general structure for each representation within each new channel. Thus we can write $V_{L, \mu L^0}^{m, m^0} = V_L^m \delta_{L, \mu L^0} \delta_{m, m^0}$. This allows us to reduce the infinite series of coupled integralequations to a limited subset that can be handled analytically. The elements of the expansion will be dominated by a single V_L^m component corresponding to the L pairing channel symmetry m , and the other components represent admixtures of channels (the smaller eigenvalues in the gap equation) with different pairing symmetry. If the gap representation is one dimensional (all representations of the D^{4h} group except E_g , which is two dimensional), then all the other V_L^m 's are set to zero

and there will only be collective modes connected with the broken $U(1)$ gauge invariance. Otherwise other collective modes can be present as well.

We now define new vertices $\hat{\gamma}_L^m(i!) = \gamma_L^m + V_L^m \hat{\gamma}_L^m(i!)$ and expand $\hat{\gamma}_L^m(i!)$ in spin quaternions,

$$\hat{\gamma}_L^m(i!) = \sum_{i=0}^3 \gamma_L^{(i)m}(i!) i; \quad (C 8)$$

The index m stands for the representations of the D^{4h} point group, and are defined through the basis functions as follows

$$\hat{\gamma}_{L=2}^m(\hat{k}) = \begin{cases} \frac{1}{2}(k_x^2 - k_y^2); & B_{1g}(\frac{+}{3})(m=1); \\ \frac{1}{6}(2k_z^2 - k_x^2 - k_y^2); & A_{1g}(\frac{+}{1})(m=2); \\ k_x k_y; & B_{2g}(\frac{+}{4})(m=3); \\ k_x k_z; & E_g(\frac{+}{5})(m=4); \\ k_y k_z; & E_g(\frac{+}{5})(m=5); \end{cases} \quad (C 9)$$

where the $\frac{+}{i}$ corresponds to the notation of Sigrist and Rice [25]. It can be shown that the coefficients $\gamma_L^{(0;1)m}$ of Pauli matrices $\sigma_{0;1}$ satisfy homogeneous equations and thus vanish while the remaining coefficients satisfy the following coupled integral equations,

$$\gamma_{L^0}^{(2)m}(i!) = \sum_{L^0 \neq 0}^X f V_{L^0}^m \gamma_{L^0}^{(2)m}(i!) C_{L, L^0}^{m \neq 0}(i!) + i(\gamma_{L^0}^{m=0} + V_{L^0}^{m=0} \gamma_{L^0}^{(3)m=0}(i!)) A_{L, L^0}^{m \neq 0}(i!) g; \quad (C 10)$$

$$\gamma_L^{(3)m}(i!) = \sum_{L^0 \neq 0}^X f i V_{L^0}^{m=0} \gamma_{L^0}^{(2)m=0}(i!) A_{L, L^0}^{m \neq 0}(i!) - (\gamma_{L^0}^{m=0} + V_{L^0}^{m=0} \gamma_{L^0}^{(3)m=0}(i!)) C_{L, L^0}^{m \neq 0}(i!) g; \quad (C 11)$$

where the functions $A; C$ are given by

$$\begin{aligned} A_{L, L^0}^{m \neq 0}(i!) &= h_L^m(\hat{k}) \gamma_{L^0}^{m=0}(\hat{k}) A(\hat{k}; i!) i; \\ C_{L, L^0}^{m \neq 0}(i!) &= h_L^m(\hat{k}) \gamma_{L^0}^{m=0}(\hat{k}) C(\hat{k}; i!) i; \end{aligned} \quad (C 12)$$

The spectral functions are defined as

$$\begin{aligned} A(\hat{k}; i!) &= i(\hat{k})! N_F \int^Z d\frac{1}{4E^2} \frac{1}{i!} \frac{2f(E)}{2E} (i! - i!); \\ C^+(\hat{k}; i!) &= N_F \int^Z d\frac{(\hat{k})^2}{2E^2} \frac{1}{i!} \frac{2f(E)}{2E} + (i! - i!); \\ C(\hat{k}; i!) &= \frac{N_F}{2} \int^Z d\frac{1}{i!} \frac{2f(E)}{2E} + (i! - i!); \end{aligned} \quad (C 13)$$

Here f is a Fermi function and $(i! - i!)$ denotes additional terms which differ only in the sign of $i!$. Analytically continuing to the real axis by letting $i! - i! + i0$, the integration can be performed analytically and we obtain

$$\begin{aligned}
A(\hat{k};!) &= (\hat{k}) F(\hat{k};!); \\
C^+(\hat{k};!) &= \frac{2}{!} \frac{\hat{k}^2}{F(\hat{k};!)}; \\
C(\hat{k};!) &= \frac{1}{V(\hat{k})} + \frac{!}{2} F(\hat{k};!);
\end{aligned} \tag{C14}$$

with

$$\begin{aligned}
F(\hat{k};!) &= \begin{cases} \frac{N_F}{(\hat{k})^2 - (!=2)^2} \arctan \frac{!}{2 \sqrt{(\hat{k})^2 - (!=2)^2}}; & \text{for } (\hat{k})^2 > (!=2)^2, \\ \frac{N_F}{2 \sqrt{(\hat{k})^2 - (!=2)^2}} i + \log \frac{!-2}{!+2} \frac{(\hat{k})^2}{(\hat{k})^2 - (!=2)^2}; & \text{for } (\hat{k})^2 < (!=2)^2, \end{cases} \tag{C15}
\end{aligned}$$

and

$$\frac{1}{V(\hat{k})} = N_F \sum_{!} \frac{d}{2E(\hat{k})} \tag{C16}$$

given by the BCS gap equation. The function F is closely related to the Tseneto function, Eq. (11).

The integral equations are still general for a charge density like vertex and the symmetry of the interaction and gap remain undetermined. We now restrict our attention to the case of d-wave interactions such that only $V_{L=2}^m \neq 0$ and other terms corresponding to interactions in higher angular momentum channels are discarded. Dropping the $L=2$ subscript by denoting $V_{L=2}^m$ by V_m and $\frac{(2;3)m}{L=2}$ by $\frac{(2;3)}{m}$, the integral equations simplify to

$$\frac{(2)}{m} (i!) = \sum_{m^0}^X fV_{m^0} [\frac{(2)}{m^0} (i!) C_{L=2;L=2}^{m^0} (i!) + i \frac{(3)}{m^0} (i!) A_{L=2;L=2}^{m^0} (i!)] + i \sum_{L^0}^X \frac{m^0}{L^0} A_{L=2;L^0}^{m^0} (i!) g; \tag{C17}$$

$$\frac{(3)}{m} (i!) = \sum_{m^0}^X fV_{m^0} [\frac{(3)}{m^0} (i!) C_{L=2;L=2}^{+m^0} (i!) + i \frac{(2)}{m^0} (i!) A_{L=2;L=2}^{m^0} (i!)] + \sum_{L^0}^X \frac{m^0}{L^0} C_{L=2;L^0}^{+m^0} (i!) g; \tag{C18}$$

These equations are still general to any d-wave pair state.

We now specially work with a B_{1g} gap, $(\hat{k}) = \frac{1}{2} (\hat{k}_x^2 - \hat{k}_y^2)$ (the $\frac{+}{3}$ representation [25]), noting that similar conclusion can be drawn for other choices of energy gaps within the $L=2$ subgroup of the D_{4h} point group. The coupled integral equations represent 10 equations for the 10 unknowns $\frac{(i)}{m}; i=2, \dots, 3g$, and the solution can be obtained by diagonalizing a 10×10 matrix. In aiding to solve the coupled integral equations, it is useful to examine the selection rules of the spectral functions $A; C$ for various subgroup indices within the $L=0;2$ channels. In particular we note that

$$\begin{aligned}
C_{L=0;L=2}^{m\pi^0} &= C_{L=2;L=2}^{4,4} = C_{L=2;L=2}^{5,5}; \quad C_{L=0;L=2}^{0\pi} = C_{L=2;L=2}^{m,2}; \\
A_{L=2;L=2}^{m\pi^0} &= A_{L=2;L=2}^{m,0} \neq f_2, 3g; \quad A_{L=2;L=2}^{1\pi} = A_{L=2;L=2}^{m,2}; \quad A_{L=2;L=2}^{2\pi} = A_{L=2;L=2}^{m,1}; \\
A_{L=0;L=0}^{0,0} &= 0; \quad A_{L=2;L=0}^{m,0} = A_{L=2;L=2}^{m,1}; \quad A_{L=2;L=2}^{4,4} = A_{L=2;L=2}^{5,5}; \quad (C19)
\end{aligned}$$

These theorems hold for the case of a B_{1g} gap only.

Handling the full gauge invariant response amounts to solving a matrix equation to identify the collective modes in each channel. Solving these equations allows one to identify the position of the collective modes by locating the zeroes of the real part of the denominator. We first simplify our notation by defining

$$\begin{aligned}
f_m^A(i!) &= \sum_{L=2;L=2}^{m\pi^0} A_{L=2;L=2}^{m\pi^0}(i!); \\
f_m^C(i!) &= \sum_{L=2;L=2}^{m\pi^0} C_{L=2;L=2}^{m\pi^0}(i!); \quad (C20)
\end{aligned}$$

We find that the $m=1$ (B_{1g}) and $m=2$ (A_{1g}) channels are coupled due to the fact that a $d_{x^2-y^2}$ energy gap squared has a component which has a finite overlap with the A_{1g} channel which is isotropic within the $x-y$ plane. Solving the integral equations we obtain for the $m=1$; (B_{1g}) and $m=2$; (A_{1g}) channels,

$$\begin{aligned}
f_1^{(2)}(i!) &= i \frac{f_1^A(i!) + V_2 A_{2,2}^{1,2}(i!) f_2^{(3)}(i!)}{1 - V_1 C_{2,2}^{1,1}(i!)}; \\
f_1^{(3)}(i!) &= \frac{f_1^C(i!) - V_2 \frac{f_1^A(i!) A_{2,2}^{1,2}(i!)}{V_1 C_{2,2}^{2,2}(i!)}}{1 + V_1 C_{2,2}^{+1,1}(i!) + \frac{V_1 V_2 \frac{A_{2,2}^{1,2}(i!) f_2^{(2)}(i!)}{V_2 C_{2,2}^{2,2}(i!)}}{1 - V_2 C_{2,2}^{2,2}(i!)} }; \\
f_2^{(2)}(i!) &= i \frac{f_2^A(i!) + V_1 A_{2,2}^{1,2}(i!) f_1^{(3)}(i!)}{1 - V_2 C_{2,2}^{2,2}(i!)}; \\
f_2^{(3)}(i!) &= \frac{f_2^C(i!) - V_1 \frac{f_1^A(i!) A_{2,2}^{1,2}(i!)}{V_1 C_{2,2}^{1,1}(i!)}}{1 + V_2 C_{2,2}^{+2,2}(i!) + \frac{V_1 V_2 \frac{A_{2,2}^{1,2}(i!) f_2^{(2)}(i!)}{V_1 C_{2,2}^{1,1}(i!)}}{1 - V_1 C_{2,2}^{1,1}(i!)} }; \quad (C21)
\end{aligned}$$

For the $m=3$ (B_{2g}) and $m=4,5$ (two E_g) channels, we find no coupling and obtain

$$\begin{aligned}
f_3^{(2)}(i!) &= i \frac{f_3^A(i!)}{1 - V_3 C_{2,2}^{3,3}(i!)}; \\
f_3^{(3)}(i!) &= \frac{f_3^C(i!)}{1 + V_3 C_{2,2}^{+3,3}(i!)}; \quad (C22) \\
f_{4,5}^{(2)}(i!) &= i \frac{f_{4,5}^A(i!) + V_{4,5} A_{2,2}^{4,4;5,5}(i!) f_{4,5}^{(3)}(i!)}{1 - V_{4,5} C_{2,2}^{4,4;5,5}(i!)};
\end{aligned}$$

$$\chi_{4;5}^{(3)}(i!) = \frac{f_{4;5}^C(i!) - V_{4;5} \frac{f_{4;5}^A(i!) A_{2;2}^{4;4;5;5}(i!)}{V_{4;5} C_{2;2}^{4;4;5;5}(i!)}}{1 + V_{4;5} C_{2;2}^{4;4;5;5}(i!) + \frac{V_{4;5} A_{2;2}^{4;4;5;5}(i!)^2}{1 - V_{4;5} C_{2;2}^{4;4;5;5}(i!)}}; \quad (C 23)$$

where $V_{4;5}$; $C_{2;2}^{4;4;5;5}$; and $A_{2;2}^{4;4;5;5}$ stand for the interactions, renormalized vertices, and spectral functions in the $m = 4;5$ channels, respectively. These equations represent the full channel-dependent renormalization of the Raman vertex due to d -wave pairing interactions.

We now are in a position to identify the collective modes in the 10 channels (5 real and 5 imaginary) by locating the zeroes of the denominator in each channel. While the functions f^A, f^C remain general and are determined by the magnitude of the Raman vertex they do not enter into the denominators of the expressions for the renormalized vertices and thus are irrelevant for the position and broadening of the collective modes. The modes located by the zeroes of the denominator are of two types, namely, massive and massless. The massless (Goldstone) modes are a consequence of the spontaneously broken $U(1)$ continuous symmetry by the interactions, while the massive (optical) modes are generated as well. Using Eqs. (C 21–C 23), in each channel we locate the zeroes of the real part of the denominator in each channel to find the position of the collective mode and evaluate the imaginary part of the denominator at the position of the collective mode to determine its broadening.

Our results are summarized in Table 1. We see that the Goldstone mode ($\omega_c = 0$) appears in the A_{1g} channel and the other modes are all massive. The B_{1g} modes lie beneath the maximum energy gap while the others appear above $2\Delta_0$. These excitonic modes are damped considerably due to the existence of quasiparticles from the presence of gap nodes which provide decay channels to damp the massive modes. This is in contrast to excitonic modes in s -wave superconductors [21,23]. However, we do observe in Table 1 that the mode position rapidly decreases to lower frequencies with depreciating residue as the coupling strength $V_m = V_{B_{1g}}$ is reduced, which is similar to the BCS case. Below a critical coupling strength $V_m = V_{B_{1g}} \approx 0.8$ the collective modes disappear altogether and thus have little impact on the low frequency behavior of the Raman correlation function for small couplings.

We now reconstruct the Raman response and determine which of the collective modes couple to the Raman vertex. Putting in Eqs. (C 21)–(C 23) into (C 1), we can express the full gauge invariant Raman response function as

$$\chi_L^m(q = 0; i!) = \sum_{m^0}^X \sum_{L^0}^X \left(\chi_{L^0}^{m^0} C_{L^0}^{m^0} (i!) + V_{m^0} \chi_{m^0}^{(3)}(i!) C_{L^0}^{m^0} (i!) - i V_{m^0} \chi_{m^0}^{(2)}(i!) A_{L^0}^{m^0} (i!) \right); \quad (C 24)$$

Taking only the $L = 0; 2$ terms of the Raman vertex into account (see Section III), we carry

out the summation over L^0 and m^0 to obtain the Ramann spectrum in each channel, and then take into account the long{range Coulomb screening via [21]

$$\chi_{sc}(q \neq 0; i!) = \frac{1}{i!} \sum_{L=0}^{\infty} \frac{C_{L,0}(i!)}{L!}; \quad (C 25)$$

where $\chi_{A,B}$ denotes Eq. (C 1) with the vertices $A(\hat{k})$ and $B(\hat{k})$, respectively.

We find that for the density channel ($L = 0$), $\chi(q \neq 0; i!) = 0$, which is a restatement of particle number conservation and bears out the gauge invariant nature of the theory. This simply restates that intercell charge fluctuations couple to the long{range Coulomb forces to be completely screened for $q \neq 0$. After lengthy but trivial algebra we obtain the compact results for the intracell fluctuation contributions. For the B_{1g} channel we obtain,

$$\chi_{B_{1g}}(i!) = 2 \left(\frac{1}{2} \right)^2 \frac{C_{B_{1g}}(i!)}{1 + V_1 C_{B_{1g}}(i!)}; \quad (C 26)$$

and for the B_{2g} channel,

$$\chi_{B_{2g}}(i!) = 2 \left(\frac{3}{2} \right)^2 \frac{C_{B_{2g}}(i!)}{1 + V_3 C_{B_{2g}}(i!)}; \quad (C 27)$$

and for the two E_g channels,

$$\chi_{E_g}(i!) = 2 \left(\frac{4}{2} \right)^2 \frac{C_{E_g}(i!)}{1 + V_{4,5} C_{E_g}(i!)}; \quad (C 28)$$

with the functions

$$C_{B_{1g}}(i!) = C_{2,2}^{+1,1}(i!) + V_2 \frac{j A_{2,2}^{1,2}(i!) j}{1 - V_2 C_{2,2}^{2,2}(i!)}; \quad (C 29)$$

$$C_{B_{2g}}(i!) = C_{2,2}^{+3,3}(i!); \quad (C 30)$$

$$C_{E_g}(i!) = C_{2,2}^{+4(5),4(5)}(i!) + V_{4(5)} \frac{j A_{2,2}^{4(5),4(5)}(i!) j}{1 - V_{4(5)} C_{2,2}^{4(5),4(5)}(i!)}; \quad (C 31)$$

These channels are unaffected by screening since the intracell fluctuations lead to no net charge transfer for these symmetries. The expression for the fully symmetric A_{1g} channel which contains both inter{and intracell fluctuations expression is much more complicated due to Coulomb screening,

$$\chi_{A_{1g}}(i!) = 2 \left(\frac{2}{2} \right)^2 \left[C_{2,2}^{+2,2}(i!) - C_{2,0}^{+2,0}(i!)^2 = C_{0,0}^{+0,0}(i!) \right] \frac{1 - \frac{0}{2} V_2 C_{A_{1g}}^0(i!)}{1 + V_2 C_{A_{1g}}(i!)}; \quad (C 32)$$

Here the functions $C_{A_{1g}}; C_{A_{1g}}^0$ are defined as

$$C_{A_{1g}}(i!) = C_{2;2}^{+2;2}(i!) + V_1 \frac{j A_{2;2}^{1;2}(i!) j}{1 - V_1 C_{2;2}^{1;1}(i!)}; \quad (C 33)$$

and

$$C_{A_{1g}}^0(i!) = C_{2;0}^{+2;0}(i!) + V_1 \frac{A_{2;2}^{1;2}(i!) A_{2;0}^{1;0}(i!)}{1 - V_1 C_{2;2}^{1;1}(i!)}; \quad (C 34)$$

Examining the structure of the denominator of Eqs. (C 26)–(C 31), we see that the massless gauge mode (Goldstone mode) in the A_{1g} channel drops out of the Raman response, and only provides screening via Eq. (C 25). The massive modes do appear in the B_{1g} and E_g channels while the massive mode found in the B_{2g} channel does not couple to a Raman probe. Linearizing the denominator around the position of the collective mode we calculate the residue Z of the mode to be $Z_{B_{1g}} = -\epsilon_c / \log(-\epsilon_c)$ and $Z_{E_g} = -\epsilon_c$, where ϵ_c is the position of the collective mode in each channel. Therefore, putting all our results together for the collective modes, we can argue that the collective modes are of little relevance to electronic Raman scattering due to the fact that 1) the modes only exist at beyond a large strong couplings threshold, 2) the residue of the modes decreases the lower the position of the collective mode, and 3) that the broadening of the collective modes are substantial.

However, of course the final state interactions themselves can affect the spectrum [21,23]. Therefore we display our results in Figs. (8a-c) for the entire spectrum in the $B_{1g}; B_{2g};$ and A_{1g} channels for different ratios of the parameter $V_m = V_{B_{1g}}$, where $V_{B_{1g}}$ is the pairing interaction of $d_{x^2-y^2}$ symmetry. The response for the E_g channels are similar to the B_{2g} case. We note that the interactions have only a minor effect on the spectra in the B_{1g} channel, only changing the cusp behavior near $2\epsilon_0$, (this demonstrates how the finite z dispersion cuts off the logarithmic singularity in Fig. 1 for the 2D Fermi surface), while leaving the peak position and low frequency behavior unchanged. The interactions have more an effect in the B_{2g} and A_{1g} channels due to the fact that the peak of the spectra are very broad. Therefore the interactions shift the peak position upwards in frequency along the top of the broad hump of the spectrum, from 1.3 to 1.5 ϵ_0 for the B_{2g} channel, and from 0.6 to 0.8 ϵ_0 in the A_{1g} channel. Again we note that the low frequency behavior remains unchanged. A similar effect is seen in the E_g channels. In particular, the massive mode in this channel is entirely damped leading to no drastic changes in the spectrum.

We close this Appendix by addressing the collective modes for a superconductor with a cylindrical (2D) Fermi surface. In a 2D system the only interactions that appear at

the $L = 2$ level are the B_{1g} and B_{2g} channels, while the A_{1g} and A_{2g} channels appear at $L = 4$. Similarly, there are no E_g channels for a system without dispersion in the z direction. Therefore, if we are only concerned with d -wave interactions and not those of higher angular momentum channels, then we can set the matrix elements $V_{A_{1g}} = V_{E_g(1;2)} = 0$ in Eqs. (C 21–C 23) and the equations simplify greatly. Since then there will be no channel mixing of the A_{1g} channels into the response, then therefore there can be no collective mode since no term appears in the denominators which has the form $1 - V_m = V_{B_{1g}}$ which arises through the function C (see Eqs. (C 21–C 23)). Therefore we can conclude that collective modes can only appear when the interactions are included in higher order L channels for a 2D system. Furthermore, the vertex corrections produce minor changes in the spectra only for the B_{1g} and B_{2g} channels. The changes are similar to the changes shown for the response functions evaluated on a spherical Fermi surface (apart from cutting off the logarithmic divergence of the B_{1g} response at the gap edge), and thus are not of major importance. We can therefore neglect the collective modes entirely and the effect of vertex corrections and simply use the bare bubble for the Raman response. This completes the purpose of the Appendix.

REFERENCES

- [1] see, e.g., J. Annett, *Adv. in Physics* 39, 83 (1990); M. Sigrist and K. Ueda, *Rev. Mod. Phys.* 63, 239 (1991); B. Batlogg, *Physica C* 169, 7 (1991); D. Pines, to appear in *Physica B*.
- [2] Z.-X. Shen et. al, *Phys. Rev. Lett.* 70, 1553 (1993); Z.-X. Shen, *J. Phys. Chem. Solids* 53, 1583 (1992).
- [3] D. A. Wollman, D. J. Van Harlingen, W. C. Lee, D. M. Ginsberg, and A. J. Leggett, *Phys. Rev. Lett.* 71, 2134 (1993); A. G. Sun, D. A. Gajewski, M. B. Maple, and R. C. Dynes, *ibid.* 72, 2267 (1994); P. Chaudhari and S.-Y. Lin, *Phys. Rev. Lett.* 72, 1048 (1994); J. R. Kirtley et. al, preprint.
- [4] J. A. Martindale et. al, *Phys. Rev. Lett.* 68, 702 (1992); P. C. Hammel, M. Takigawa, R. H. Heiner, Z. Fisk and K. C. Ott, *Phys. Rev. Lett.* 63, 1992 (1989); W. N. Hardy, D. A. Bonn, D. C. Morgan, R. Liang and K. Zhang, *Phys. Rev. Lett.* 70, 3999 (1993); Z. Ma et. al, *Phys. Rev. Lett.* 71, 781 (1993); S. Anlage et. al, *Phys. Rev. B* 44, 9764 (1991).
- [5] J. Kosztin and A. Zawadowski, *Solid State Commun.* 78, 1029 (1991).
- [6] P. B. Allen, *Phys. Rev. B* 13, 1416 (1976).
- [7] T. P. Devereaux, D. Einzel, B. Stadlober, R. Hackl, D. H. Leach, and J. J. Neumeier, *Phys. Rev. Lett.* 72, 396 (1994); *ibid.* 72, 3291 (1994).
- [8] S. L. Cooper and M. V. Klein, *Comments Condens. Mat. Phys.* 15, 19 (1990).
- [9] S. L. Cooper, M. V. Klein, B. G. Pazol, J. P. Rice and D. M. Ginsberg, *Phys. Rev. B* 37, 5920 (1988); R. Hackl, in *Electronic Properties of High- T_c Superconductors and Related Compounds*, eds. H. Kuzmany, M. M ehling and Z. Fisk, Springer Series in Solid-State Sciences Vol. 99 (Springer, Berlin, 1991).
- [10] S. L. Cooper, F. Slakey, M. V. Klein, J. P. Rice, E. D. Bukowski and D. M. Ginsberg, *Phys. Rev. B* 38, 11934 (1988).
- [11] R. Hackl, W. Glaser, P. Muller, D. Einzel and K. Andres, *Phys. Rev. B* 38, 7133 (1988).
- [12] T. Stauffer, R. Nemetschek, R. Hackl, P. Muller and H. Veith, *Phys. Rev. Lett.* 68, 1069 (1992).
- [13] R. Nemetschek, O. V. Misochko, B. Stadlober and R. Hackl, *Phys. Rev. B* 47, 3450 (1993).

- [14] Important information can also be obtained from the renormalization of low lying phonons as the gap opens below T_c (see e.g. C. Thom sen, in *Light Scattering in Solids VI*, edited by M. Cardona and G. Guntherodt (Springer, Berlin, 1991)). The theory of the polarization dependence of the phonon renormalization in a $d_{x^2-y^2}$ superconductor has been recently given in Ref. [36].
- [15] O. Betbedet-Matibet and P. Nozières, *Ann. Phys. (N.Y.)* 51, 392 (1969).
- [16] D. Vollhardt and P. Wölfe, *The Superfluid Phases of ^3He* , Taylor & Francis, London, 1990.
- [17] T. T suneto, *Phys. Rev.* 118, 1029 (1960).
- [18] P. J. Hirschfeld, P. Wölfe, J. A. Sauls, D. Einzel, and W. O. Putikka, *Phys. Rev. B* 40, 6695 (1989).
- [19] D. Pines and P. Nozières, *The Theory of Quantum Liquids*, W. A. Benjamin, New York, 1966.
- [20] P. J. Hirschfeld and D. Einzel, *Phys. Rev. B* 47, 8837 (1993).
- [21] M. V. Klein and S. B. Dierker, *Phys. Rev. B* 29, 4976 (1984); H. Monien and A. Zawadowski, *Phys. Rev. B* 41, 8798 (1990).
- [22] A. A. Abrikosov and V. M. Genkin, *Zh. Eksp. Teor. Fiz.* 65, 842 (1973) [*Sov. Phys. JETP* 38, 417 (1974)].
- [23] T. P. Devereaux, *Phys. Rev. B* 47, 5230 (1993).
- [24] T. P. Devereaux, preprint.
- [25] M. Sigrist and M. Rice, *Z. Phys. B - Condensed Matter* 68, 9 (1987).
- [26] see, e.g., J. Yu and A. J. Freeman, *J. Phys. Chem. Solids* 52, 1351 (1991); A. Zawadowski, *Physica Scripta T* 27, 66 (1989).
- [27] W. E. Pickett, *Rev. Mod. Phys.* 61, 433 (1989).
- [28] T. P. Devereaux, preprint.
- [29] M. Tinkham, *Group Theory and Quantum Mechanics*
- [30] This indicates that the energy gap can only be identified with the peak position in the B_{1g}

channel, and the temperature dependence of the peak position will most closely follow its true form only in this channel. However, it is to be noted that impurities will also change the position of the peak away from $2\phi_0$ even in this channel as well (see Ref. [23]), making the identification of the gap from the peak maximum less precise.

- [31] A. Homann and G. Guntherodt, private communication.
- [32] G. Kotliar, Phys. Rev. B 37, 3664 (1988); R. Joynt, Phys. Rev. B 41, 4271 (1990); see also Q. P. Li, B. E. C. Koltenbah, and R. Joynt, Phys. Rev. B 48, 437 (1993).
- [33] S. Chakravarty, A. Sudbo, P. W. Anderson, and S. Strong, Science 261, 337 (1993).
- [34] J. C. Camuzano, private communication.
- [35] A. Virosztek and J. Ruvalds, Phys. Rev. B 45, 347 (1992).
- [36] T. P. Devereaux, A. Virosztek, and A. Zawadowski, preprint; T. P. Devereaux, to appear in Phys. Rev. B.
- [37] N. D. Mermin, Phys. Rev. B 1, 2362 (1970).
- [38] D. Einzel and P. J. Hirschfeld, Physica B 194-196, 1363 (1994).
- [39] Dietrich Einzel, unpublished.
- [40] V. Emery and D. Cheng, Phys. Rev. Lett. 21, 533 (1968).
- [41] D. S. Hirashina and H. Namaiawa, Journ. of Low Temp. Phys. 73, 137 (1988).
- [42] V. J. Emery, Synth. Met. 13, 21 (1986); K. Miyake, S. Schmitt-Rink, and C. M. Varma, Phys. Rev. B 34, 6554 (1986); D. J. Scalapino, E. Loh, and J. E. Hirsch, Phys. Rev. B 34, 5370 (1986); P. Monthoux, A. V. Balatsky and D. Pines, Phys. Rev. Lett. 67, 3449 (1991).
- [43] R. E. Prange, Phys. Rev. 129, 2495 (1963).
- [44] K. Itai, Phys. Rev. B 45, 707 (1992).

FIGURES

FIG .1. Electronic Raman response functions evaluated for $d_{x^2-y^2}$ pairing on a cylindrical Fermi surface for various symmetries as indicated. All vertices have been set equal to 1.

FIG .2. Ratio of the low frequency Raman response in the superconductor with $d_{x^2-y^2}$ pairing to the normal metal for the temperatures indicated. Note the slow decrease of the A_{1g} and B_{2g} channels with temperature.

FIG .3. Response functions for various symmetries for s -id pairing with $\mu_s = \mu_d = 0.25$. All vertices are set to 1.

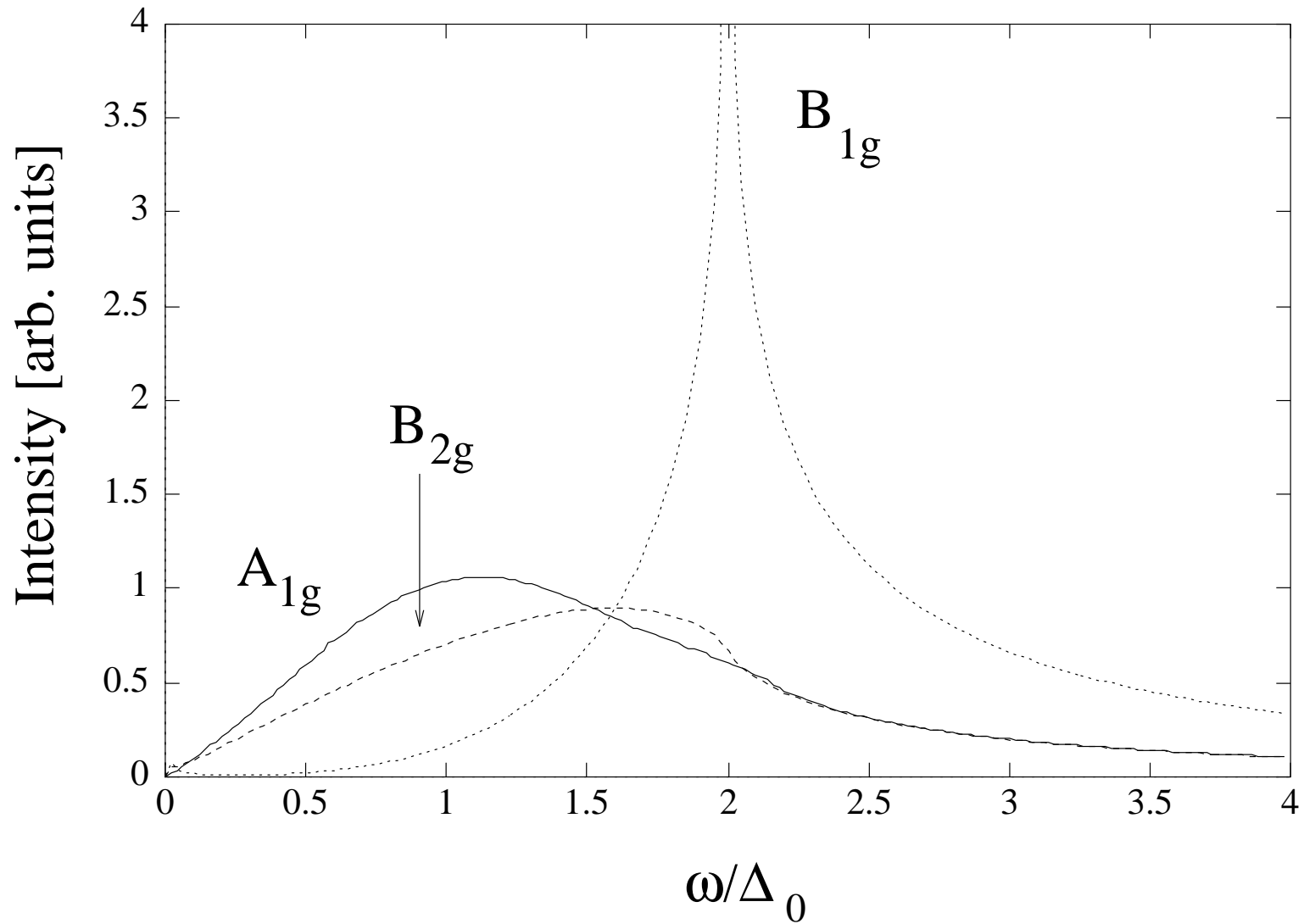
FIG .4. Response functions for various symmetries for anisotropic s -wave pairing with $\mu_0 = \mu_1 = 0.25$. All vertices are set to 1.

FIG .5. Comparison of the theory to the experimental data taken on BSCCO from Ref. [12] using $d_{x^2-y^2}$ pairing. The parameters used are defined in the text.

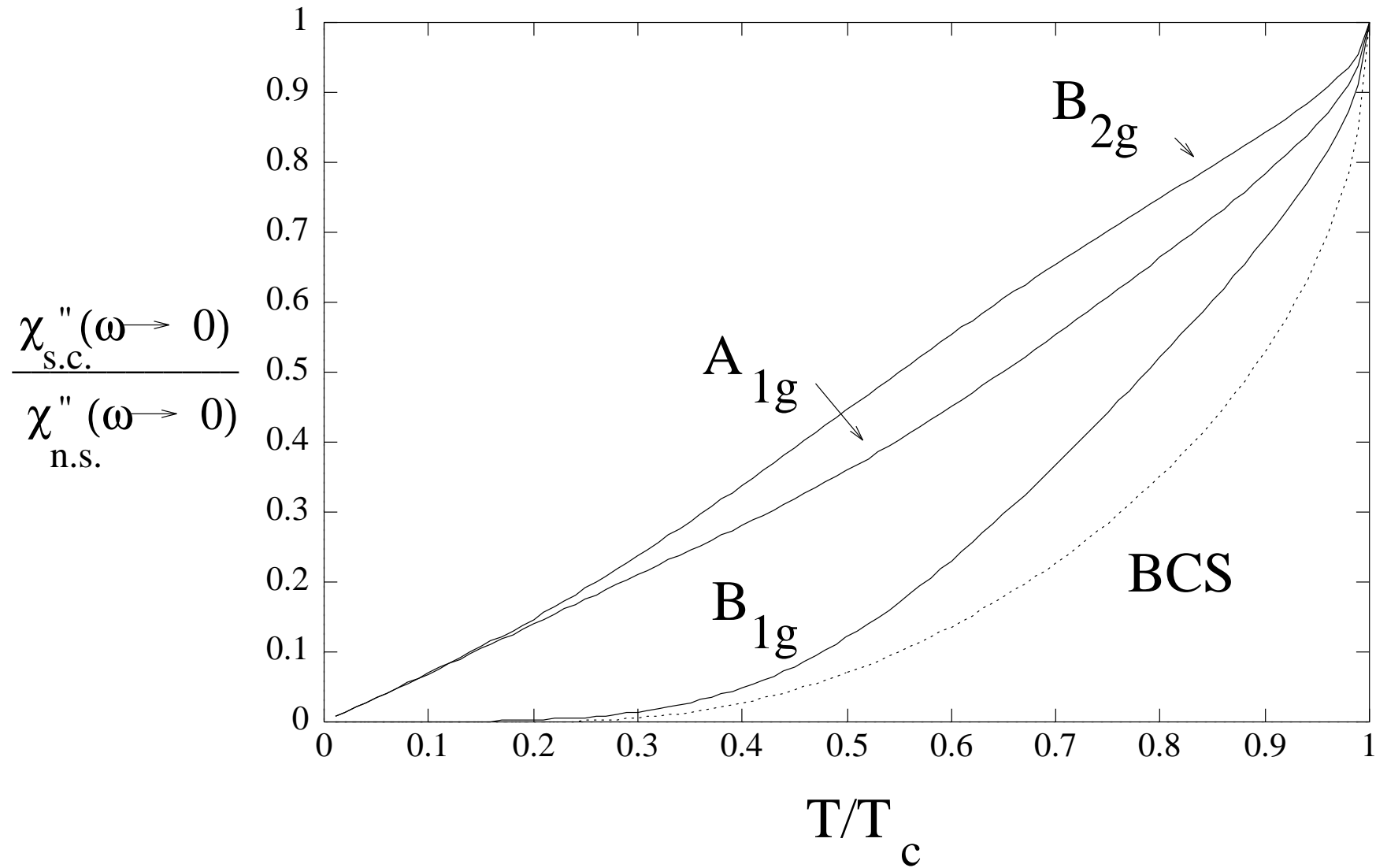
FIG .6. Comparison of the theory to the experimental data taken on YBCO using $d_{x^2-y^2}$ pairing from Ref. [11]. The parameters used are defined in the text.

FIG .7. Comparison of the theory to the experimental data taken on single layer Thallium cuprate using $d_{x^2-y^2}$ pairing from Ref. [13]. The parameters used are defined in the text.

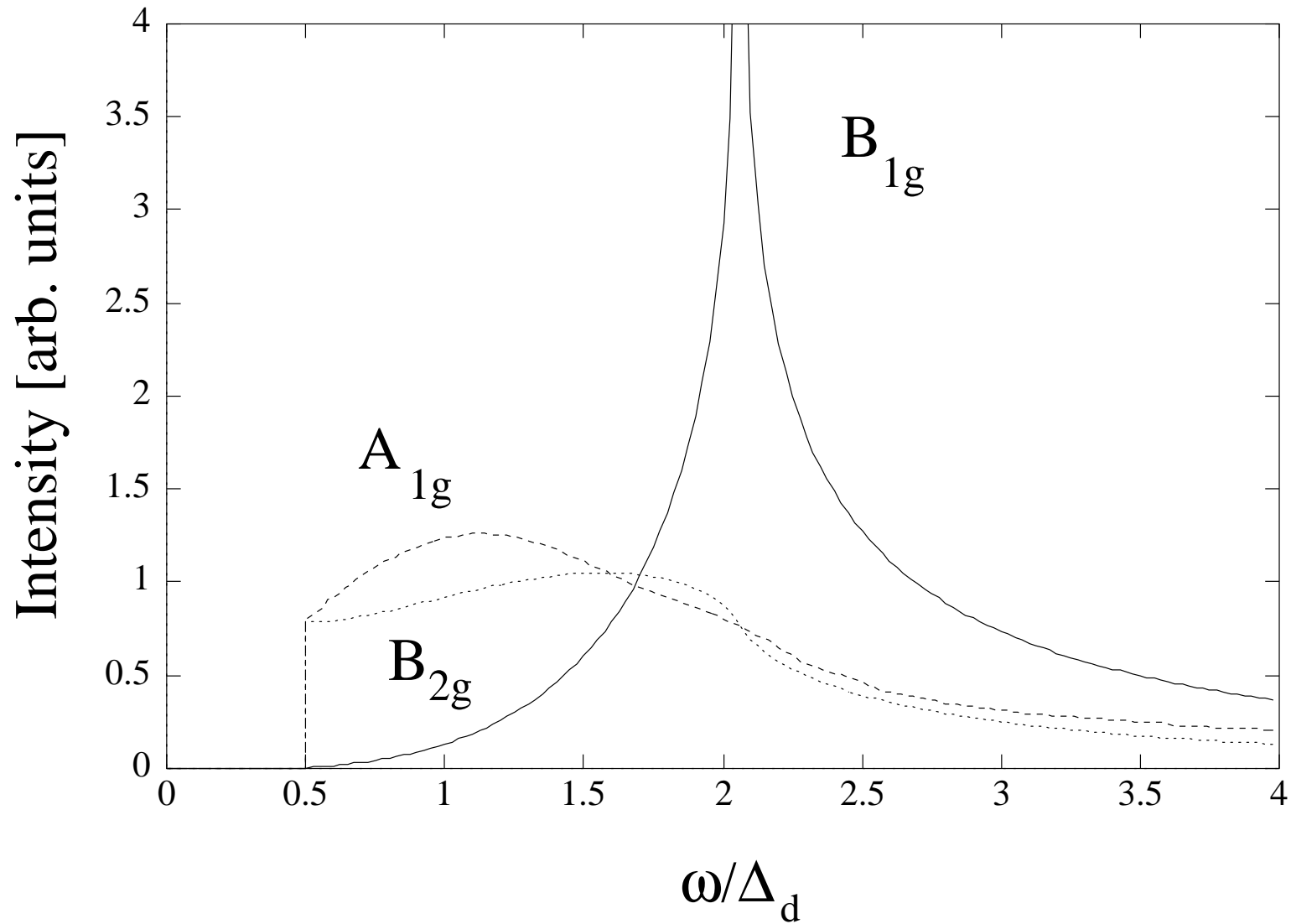
FIG .8. Effect of vertex corrections on the Raman response evaluated for $d_{x^2-y^2}$ pairing on a spherical Fermi surface for (a) B_{1g} , (b) B_{2g} , and (c) A_{1g} channels (using $\mu_0 = \mu_2 = 2$, other vertices set equal to 1). The E_g results look identical to the B_{2g} spectra. Here we have used $V_{B_{1g}} = 0.2$, and the values of $V_m = V_{B_{1g}}$ are indicated in the upper right hand corner of the Figure.



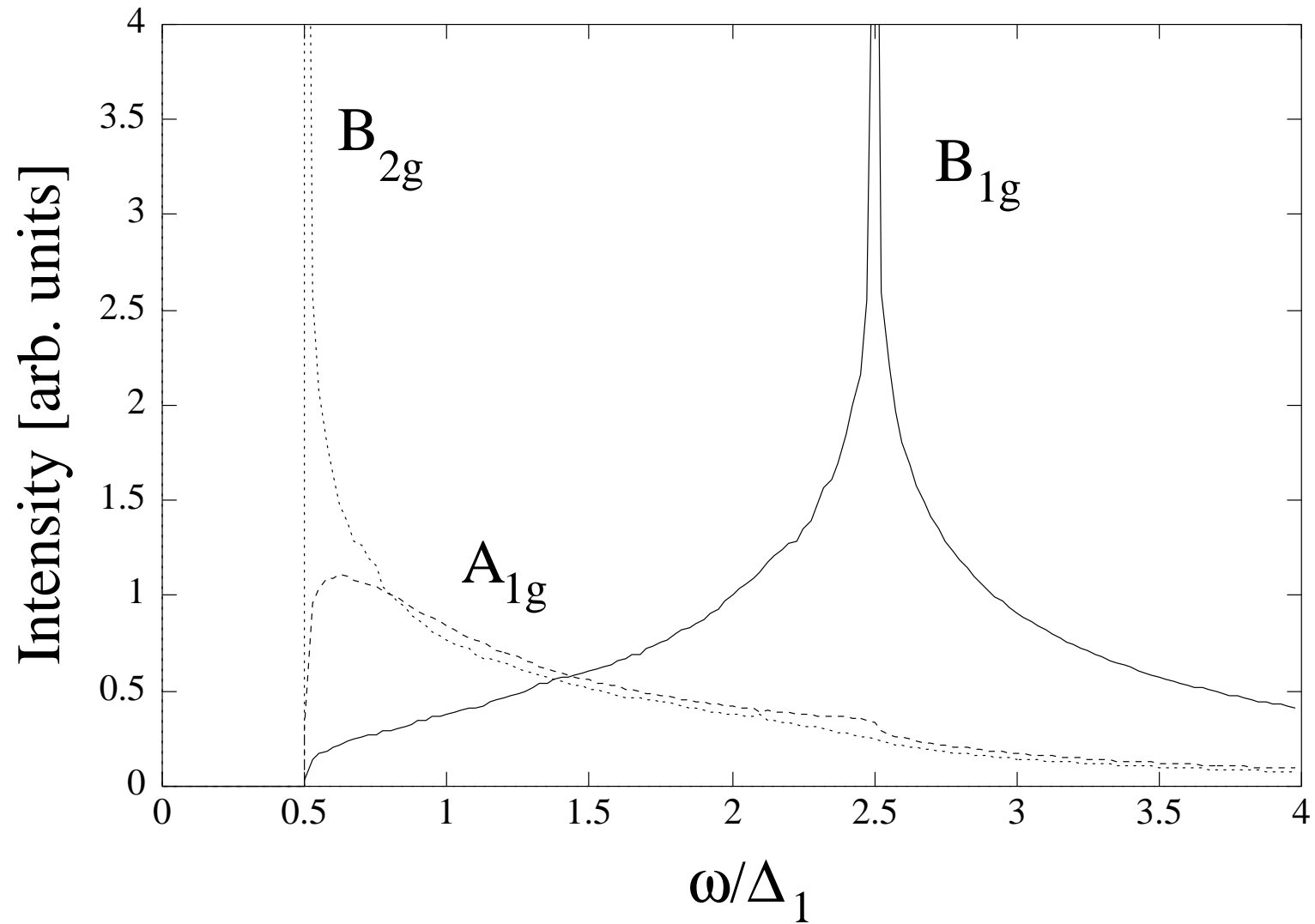
Devereaux and Einzel, Fig. 1.



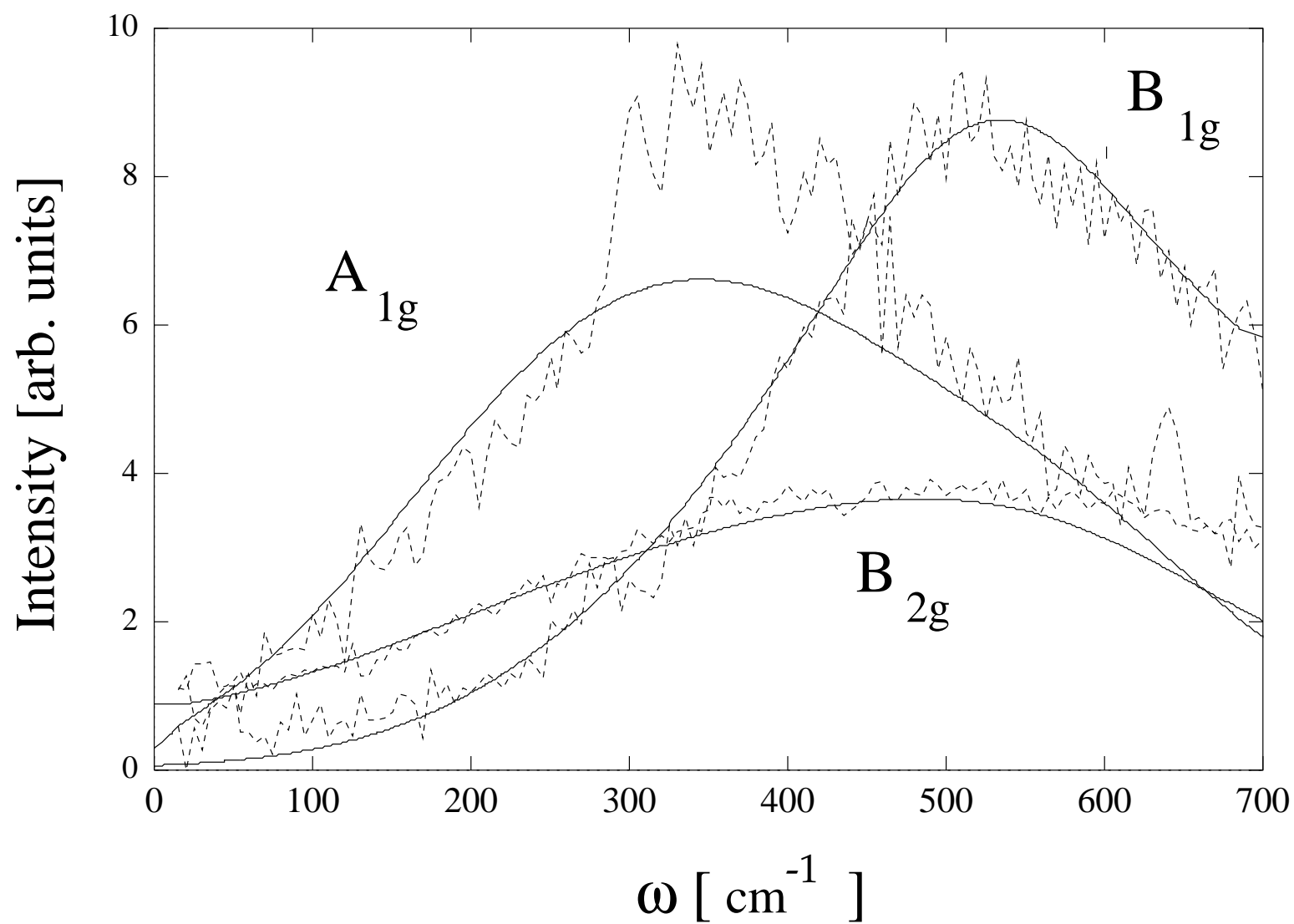
Devereaux and Einzel, Fig. 2.



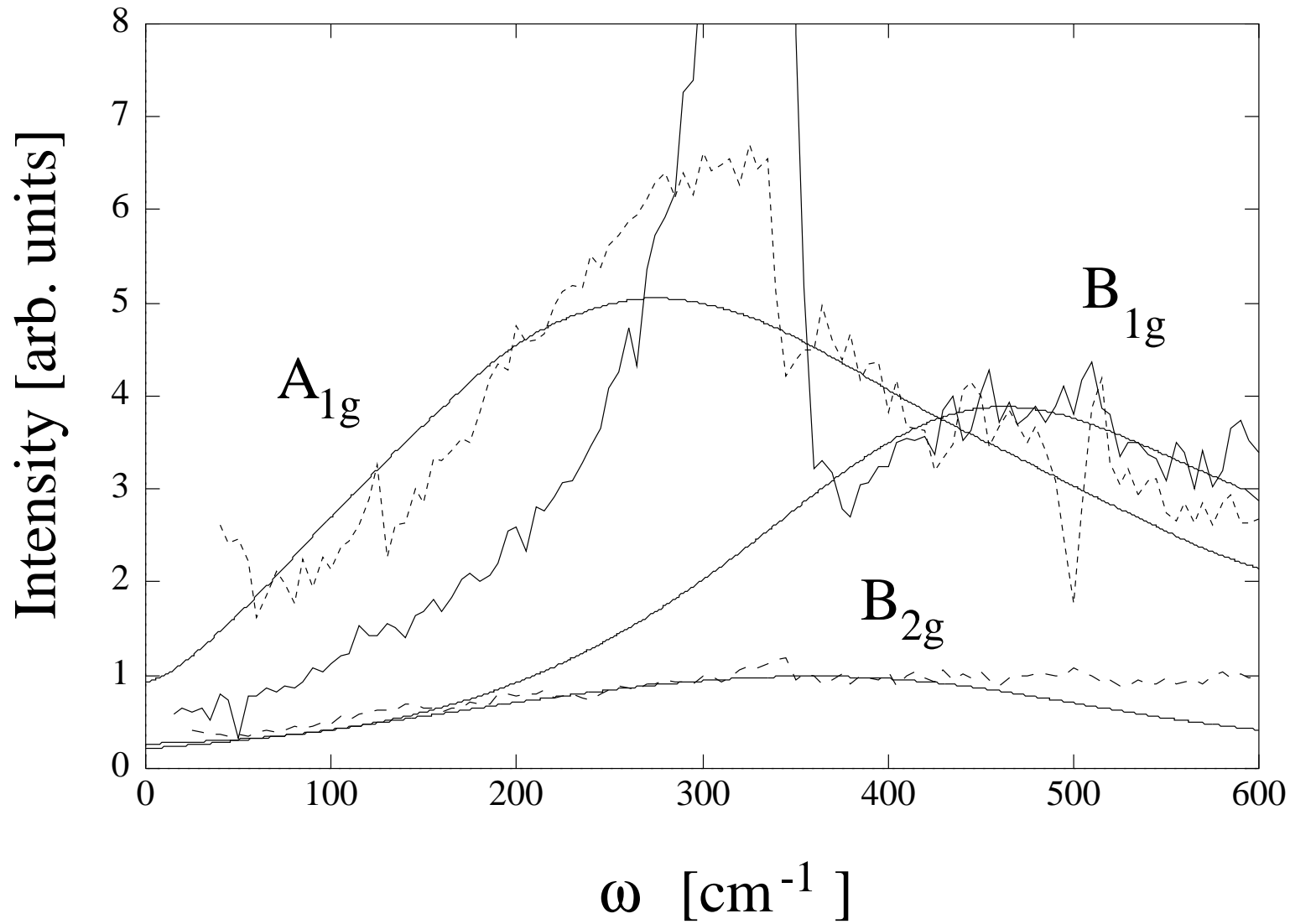
Devereaux and Einzel, Fig. 3.



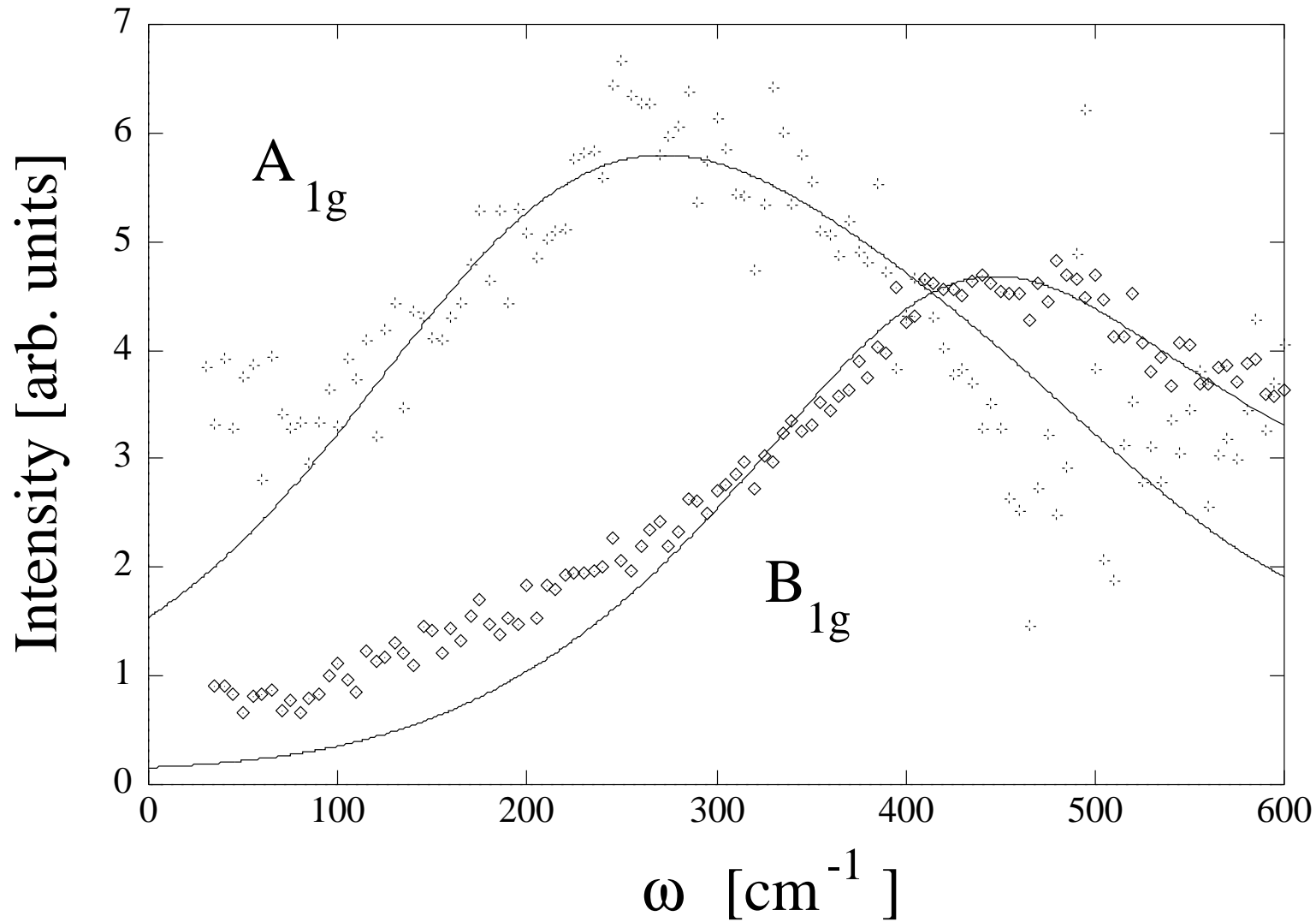
Devereaux and Einzel, Fig. 4.



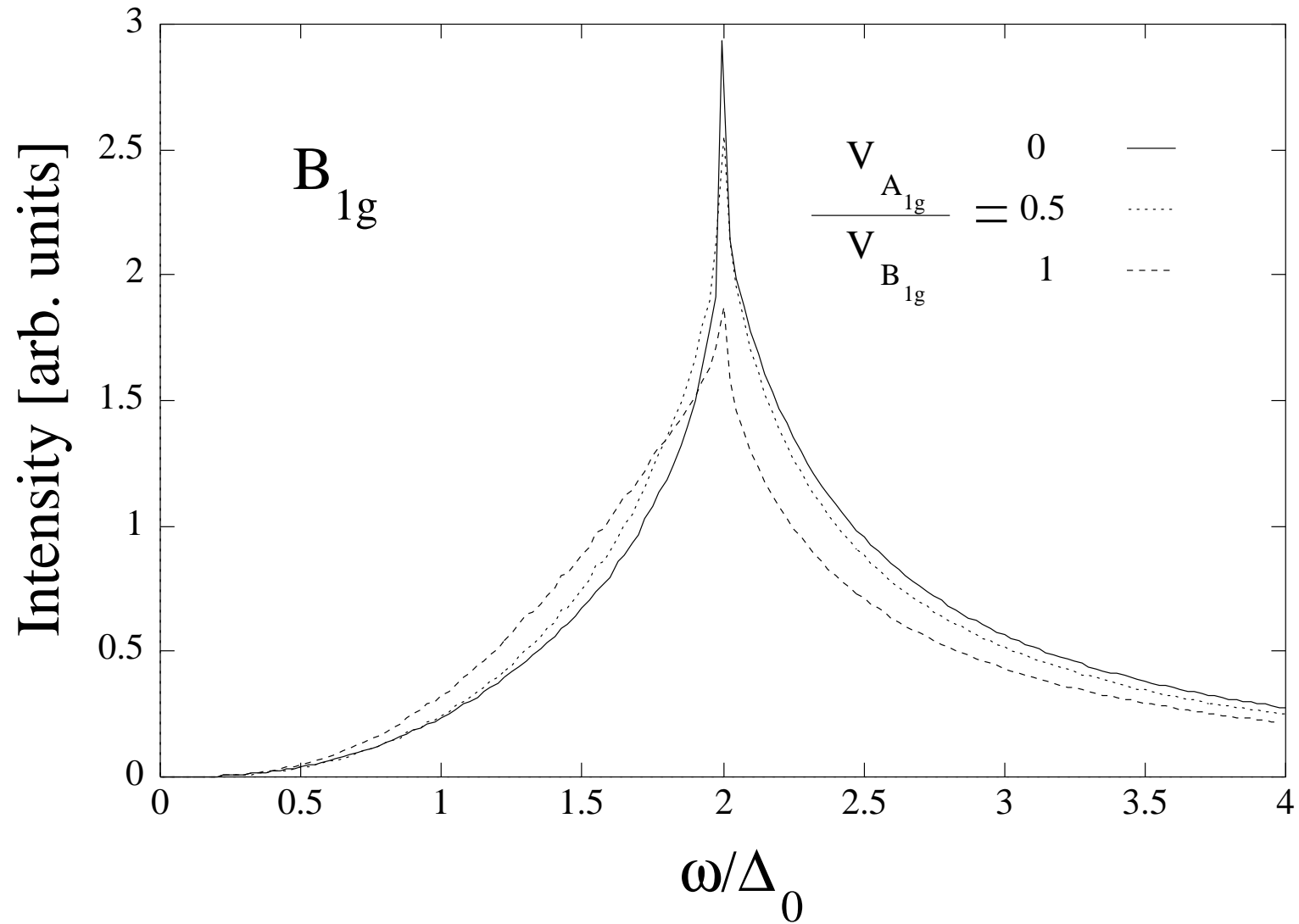
Devereaux and Einzel, Fig. 5.



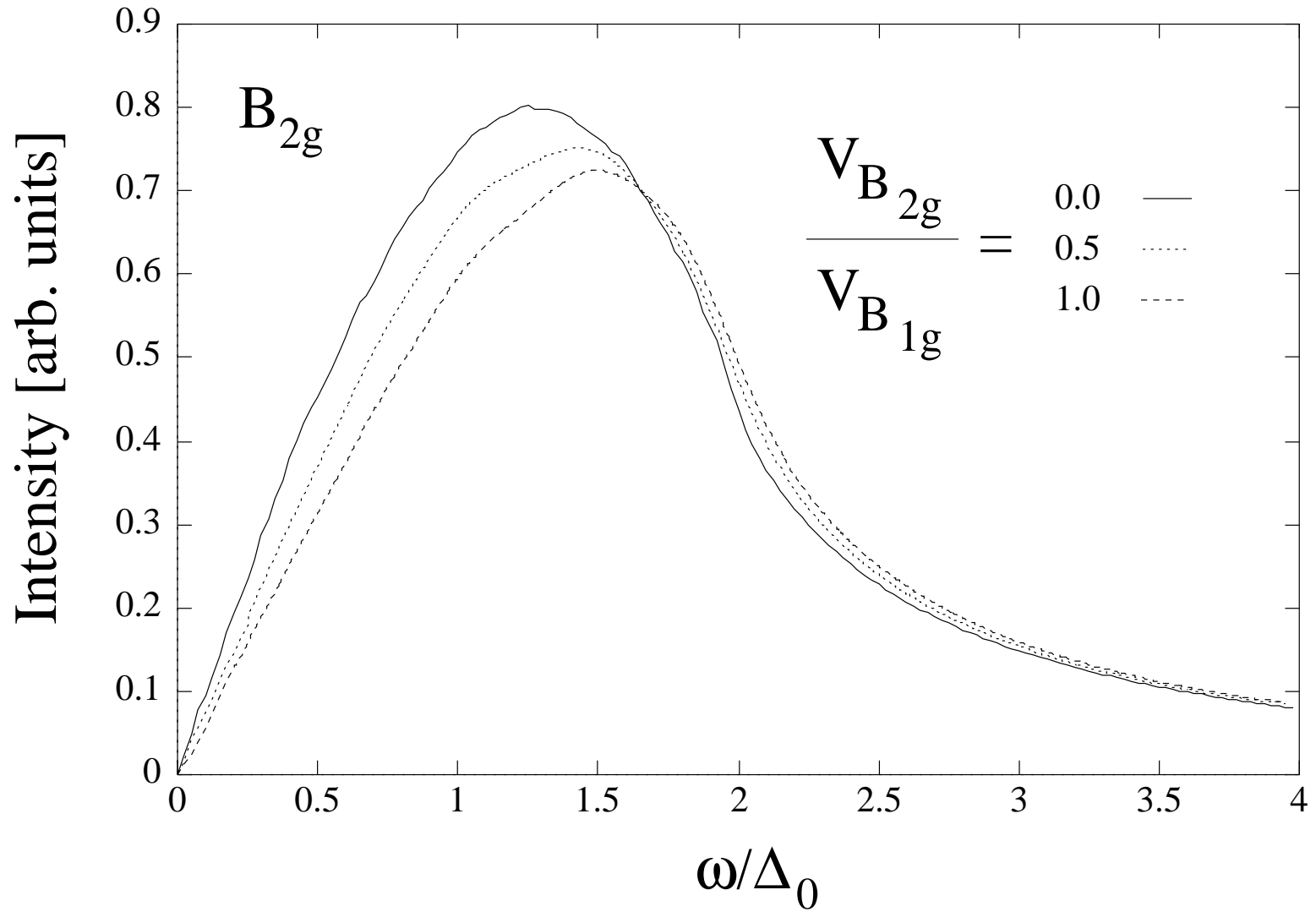
Devereaux and Einzel, Fig. 6.



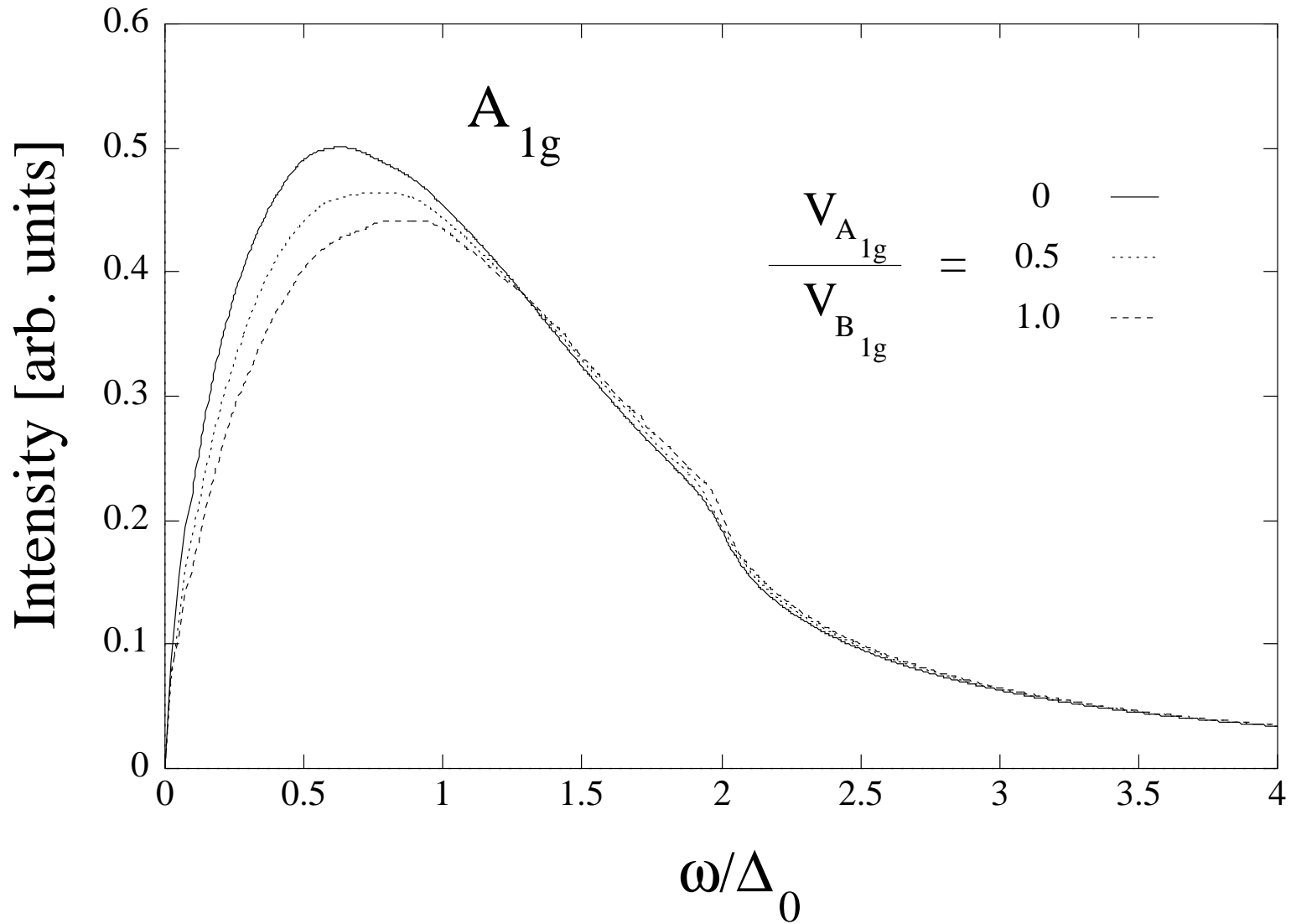
Devereaux and Einzel, Fig. 7.



Devereaux and Einzel, Fig. 8a.



Devereaux and Einzel, Fig. 8b.



Devereaux and Einzel, Fig. 8c.

TABLE 1

Position $\sqrt{s_c}=2 \text{ }_0$ and broadening $\Gamma_c=2 \text{ }_0$ of the pole in $\pi_m^{(2;3)}$ for each channel.

\sqrt{s}	$\pi_1^{(2)} (\pi_{1g})$	$\pi_1^{(3)} (\pi_{1g})$	$\pi_2^{(2)} (\pi_{1g})$	$\pi_2^{(3)} (\pi_{2g})$	$\pi_3^{(2)} (\pi_{2g})$	$\pi_3^{(3)} (\pi_{2g})$	$\pi_{4;5}^{(2)} (\pi_g)$	$\pi_{4;5}^{(3)} (\pi_g)$
$\frac{\sqrt{s_c}}{2 \text{ }_0}$	0.87	0.83	Goldstone	Goldstone	1.16	1.16	1.15	1.09
$\frac{\Gamma_c}{2 \text{ }_0}$	0.17	0.20			0.23	0.23	0.23	0.22